Available on the CERN CDS information server **CMS PAS SUS-14-012**

CMS Physics Analysis Summary

Contact: cms-pag-conveners-susy@cern.ch 2015/01/15

Supersymmetry discovery potential in future LHC and HL-LHC running with the CMS detector

The CMS Collaboration

Abstract

The search for supersymmetry (SUSY) is a major goal of the LHC physics program. The number of SUSY scenarios is large, and both high luminosity data samples and the full set of CMS detector capabilities are required to provide sensitivity to the broad range of signatures, cross sections, and decay branching fractions that can arise. If evidence for a spectrum of new particles is discovered, an extensive program of measurements will be required to determine its properties. In this document, results are presented from a set of studies that address key questions related to the anticipated program of SUSY searches, assuming integrated luminosities from 300 fb^{-1} (LHC Run 2+3) to 3000 fb^{-1} (High Luminosity LHC). Natural SUSY models, which are motivated by the puzzle of how the low value of the Higgs mass is stabilized (the gauge hierarchy problem), are one of the most important areas of investigation. Three full-spectrum natural SUSY scenarios are considered in detail, as well as other scenarios that lead to challenging experimental signatures, such as compressed mass spectra. For some studies, simplified model spectra (SMS) are used to study scenarios in which a small number of SUSY particles dominate the event sample for a particular experimental signature. Using these complementary approaches, results are presented on the sensitivities of measurements with a varying number of jets, b-tagged jets, and leptons, and with a variety of different kinematic variables. These studies, together with results from previous investigations, demonstrate the tremendous potential for discovering and elucidating SUSY with the CMS detector in future LHC running.

1 Introduction

Supersymmetry (SUSY) [1–6] is one of the best motivated theories for physics beyond the standard model (SM). First, SUSY provides a candidate particle, the lightest supersymmetric particle (LSP), that may account for all or part of the astrophysical dark matter. For example, in the minimal supersymmetric standard model (MSSM), the lightest neutralino, designated $\widetilde{\chi}_1^0$, is a superposition of the spin-1/2 superpartners of the neutral gauge and Higgs bosons, and it can in principle satisfy the constraints from indirect dark matter observations. Second, if a SUSY particle spectrum is present, the three running gauge couplings of the SM interactions can converge at a common high energy, a requirement for gauge unification. Finally, the discovery of a Higgs boson by the CMS and ATLAS experiments has given new urgency to the gauge hierarchy problem. Assuming that the Higgs boson is a fundamental scalar particle, its mass is extremely sensitive to short distance quantum corrections. Without some kind of new physics that compensates for these effects, the Higgs mass would be pulled up to the Planck scale, barring a coincidental near-perfect cancellation of the bare Higgs mass parameter and the enormous shift induced by quantum corrections. A broad class of SUSY scenarios, known as natural models [7], can stabilize the Higgs boson mass through additional contributions involving diagrams with the scalar superpartner, $\widetilde{\mathrm{t}}$, of the top quark, as well as other SUSY particles.

If evidence for one or more new particles is discovered, an extensive program of measurements will be required to determine whether they are indeed SUSY partners of SM particles, and to address even more challenging issues such as the mechanism of SUSY breaking. The range of SUSY scenarios is broad, and both high luminosity data samples and the full set of CMS detector capabilities will be needed to provide sensitivity to the signatures, cross sections, and decay branching fractions of interest. Because of the complexity of the SUSY spectrum and the associated decay processes, such a program would likely extend for many years, as was the case for studies of the SM hadron spectrum.

In the coming years, the LHC will run at a center-of-mass energy of 13 TeV and subsequently at 14 TeV, providing access to higher – yet untested – SUSY masses during Run 2 and Run 3 with an accumulated luminosity of up to $300\,\mathrm{fb}^{-1}$ by 2023. Beyond this, the high-luminosity LHC (HL-LHC), which is planned to start with an upgraded detector in 2025, will deliver up to $3000\,\mathrm{fb}^{-1}$ of integrated luminosity over the following ten years.

Previous studies [8–11] by CMS and ATLAS have concentrated on SUSY search sensitivities for particle discovery. The studies presented below consider possible follow-up measurements with up to $3000\,\mathrm{fb}^{-1}$. The specific example models were chosen to illustrate the physics potential for normal as well as compressed spectra, and for various different assumptions on the nature of the LSP and the weakly interacting SUSY sector. We consider not only the discovery sensitivity, but also how, in the event of a discovery, the pattern of signals and the associated kinematic distributions can provide many clues to understanding the nature of the underlying particle spectrum. From these 'discovery stories' it is clear that the full HL-LHC data sample will provide critical information, even if discoveries are made much earlier.

We also investigate the discovery reach for direct chargino-neutralino production in the WZ and WH final states using simplified models [12, 13]. The cross section of direct electroweak neutralino-chargino production is more than two orders of magnitude smaller than the one for strongly produced SUSY particles of comparable masses. Therefore, searches for direct electroweak production especially profit from the high-luminosity upgrade of the LHC. For the search in the WH final state, we study the degradation of the detector performance for the case

of a reduced upgrade scenario where only the pixel detector would be replaced after 300 fb^{-1}. In this scenario, radiation damage will affect most observables relevant to SUSY searches, resulting in negligible gain in discovery sensitivity, in spite of the huge increase in integrated luminosity to 3000 fb^{-1}.

An overview over the results obtained by the 8 TeV analyses is given in Section 2, followed by a short introduction to the LHC and CMS upgrade plans in Section 3. The models and analysis overview are discussed in Section 4. The analysis strategy concerning the event simulation, systematic uncertainties, and significance calculation is described in Section 5, followed by Sections 6 to 13 describing the different analyses and their significances for the different models, including a discussion of the gain from extending the luminosity up to 3000 fb^{-1}. The discovery stories are summarized in Section 14, followed by the conclusions in Section 15.

2 Status of SUSY searches

With the analysis of about 20 fb^{-1} of data recorded at a center-of-mass energy of 8 TeV, the SUSY parameter space has been tested in various ways. The results have mainly been interpreted in simplified models that describe the on-shell pair-production of specific SUSY particles and their decay to SM particles and the lightest SUSY particle (LSP), often assuming a branching fraction of 100% for the investigated decay. In addition, the individual analyses are re-interpreted in the parameter space of a phenomenological minimal supersymmetric model (pMSSM) [14–16].

At the LHC, the cross sections for colored particle production are higher than for electroweak production of superpartners of comparable mass, yielding a higher mass reach for colored supersymmetric particles (sparticles). In case of gluino ($\tilde{g}$) production, with $\tilde{g} \to t\bar{t}\tilde{\chi}_1^0$, gluino masses below 1.3 TeV for neutralino masses up to 500–600 GeV are excluded [17]. The exclusion for gluino decays to the first two generations of quarks extends to gluino masses up to about 1.3 TeV as well [18]. Direct production of the first two generations of squarks ($\tilde{q}$) has also been tested, with $\tilde{q} \to q\tilde{\chi}_1^0$, excluding squarks up to 900 GeV for neutralino masses up to 300 GeV. If only one of these squarks is light, squark masses of up to 500 GeV are excluded for neutralino masses of up to 100 GeV [18]. The production of electroweak sparticles, especially chargino-neutralino ($\tilde{\chi}_1^{\pm}\tilde{\chi}_2^0$) production, has been tested with 8 TeV analyses as well. The $\tilde{\chi}_1^{\pm}$ and $\tilde{\chi}_2^0$ are assumed to be mass-degenerate and are excluded up to about 700 GeV for $\tilde{\chi}_1^0$ masses of about 300 GeV, depending on the assumptions on the rest of the SUSY particle spectrum [19].

Based on the 8 TeV analyses, studies have been performed for several simplified models, in order to predict the possible discovery sensitivity at 300 fb^{-1} and 3000 fb^{-1} [9]. A summary of projected discovery sensitivities is given in Fig. 1. The mass reach for gluino-gluino production can be extended by about 20% up to about 2.2 TeV when the luminosity is increased from 300 fb^{-1} to 3000 fb^{-1} [9]. The sensitivity to chargino-neutralino production will be increased by 30–50%, depending on the decay channel, up to 950 GeV, probing the most interesting region where the masses of the light electroweak sparticles are expected in the framework of natural SUSY models.

3 LHC and CMS upgrade configurations

We investigate the discovery reach for several representative SUSY searches with 3000 fb^{-1} of 14 TeV pp collisions as expected with the HL-LHC. Such a high integrated luminosity exceeds the initial design value for the CMS detector by a factor of ten and can only be reached after a second ("Phase II") upgrade of the CMS experiment during the LHC running at a center-of-

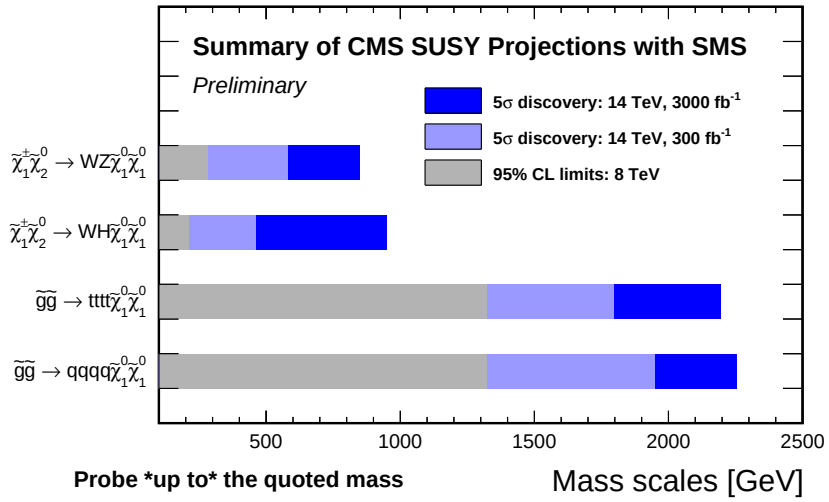

Figure 1: Mass reach of searches for supersymmetry from selected 8 TeV results (masses excluded at 95% CL) and from projections for 14 TeV running with 300 and 3000 fb^{-1} (highest masses for 5σ observation). Simplified model spectra (SMS) topologies are used for the interpretations in each case. The processes listed are the direct electroweak production of $\widetilde{\chi}_1^{\pm}\widetilde{\chi}_2^0$ pairs decaying into the $WZ\widetilde{\chi}_1^0\widetilde{\chi}_1^0$ and $WH\widetilde{\chi}_1^0\widetilde{\chi}_1^0$ final states; gluino pair production with $\widetilde{g} \rightarrow t\bar{t}\widetilde{\chi}_1^0$; and gluino pair production with $\widetilde{g} \rightarrow q\bar{q}\widetilde{\chi}_1^0$.

mass energy of 14 TeV. While the LHC design instantaneous luminosity is 1×10^{34} $\text{cm}^{-2}\text{s}^{-1}$, the nominal scenario of the high luminosity LHC is to operate at a leveled luminosity of 5×10^{34} $\text{cm}^{-2}\text{s}^{-1}$.

The primary goal of the Phase II upgrade program is to maintain the excellent performance of the Phase I detector under these challenging conditions throughout the extended operation of the HL-LHC. Performance projections based on a combination of detailed measurements using the data taken in the experiment throughout the period 2010–2012 and the exposure of test components to radiation levels matching anticipated HL-LHC show that the tracker and the endcap calorimeters will suffer significantly from radiation damage after 300–500 fb^{-1}, and a plan for their major upgrade is being developed.

This upgrade is designed to mitigate performance issues associated with high pileup (PU), which is most pronounced in the inner and forward detector regions. The tracker granularity can be increased to maintain the excellent tracking efficiency in order to enable the determination of the original proton-proton collision points for all charged particles. New endcap calorimeter configurations will also provide the opportunity to optimize segmentation and improve energy resolution, particularly for jets.

4 Full-spectrum SUSY models used for benchmark studies

In this section we discuss five benchmark full-spectrum SUSY models that are used for studies presented in this document. The SUSY particle mass spectra in these models are shown in Fig. 2 and further details of these models are presented in Appendix A. These five SUSY models contain production and decay channels that could be discovered with integrated luminosity of either up to 300 fb^{-1} or up to 3000 fb^{-1}. The first three models are motivated by naturalness (e.g. Ref. [7]), and differ by the mass of the sleptons and also by the composition of neutralinos and charginos, which are mixture of binos, winos, and higgsinos. Depending on the nature of these

weakly interacting SUSY particles, the decay of the higher-mass colored SUSY particles differs dramatically. Two other models contain coannihilation scenarios, which are motivated by their prediction of the relic density due to coannihilation of either the $\widetilde{t}_1$ and the $\widetilde{\chi}_1^0$, or the $\widetilde{\tau}_1$ and the $\widetilde{\chi}_1^0$.

The models are calculated using SUSPECT 2.41/2.43 [20] or SOFTSUSY 3.4.0 [21] in combination with SUSY-HIT 1.3b/3.4 [22]. These models specified in the SUSY Les Houches Accord (SLHA) format are processed with MADGRAPH 5 [23, 24]. The resulting Les Houches Event (LHE) files are then run through PYTHIA 6.4 [25] for fragmentation and hadronization and DELPHES 3.0.10 [26] for detector simulation.

4.1 Natural models (NM)

The three natural pMSSM models differ mainly in the masses of the sleptons and in the masses and compositions of the neutralinos and charginos (also referred to as ewkinos), which are governed by the gauge eigenstate mass terms, M_1, M_2, and μ. All three models have a relic density that is smaller than the recent measurement based on the Planck and WMAP data of 0.1199 ± 0.0027 [27, 28] and are thus not overclosing the universe. Depending on their mass hierarchy, we can distinguish between bino-like ($\mu > M_2 > M_1$), higgsino-like ($M_2 > M_1 > \mu$), and wino-like (or co-NLSP, with $\mu > M_1 > M_2$) flavor of the $\widetilde{\chi}_1^0$.

In all three models the gluino with a mass of about 1.7 TeV should be discoverable with less than $300\,\text{fb}^{-1}$ of integrated luminosity. The squarks of the third generation with masses of approximately 1 TeV are either produced in the gluino decay or in direct pair production. Their discovery depends on the model-specific decay pattern. The first- and second-generation squarks have a mass of about 3 TeV.

The first model, called NM1, has a bino-like $\widetilde{\chi}_1^0$, wino-like $\widetilde{\chi}_1^\pm$ and $\widetilde{\chi}_2^0$, and higgsino-like $\widetilde{\chi}_2^\pm$ and $\widetilde{\chi}_{3,4}^0$. The slepton mass is in between the (mass-degenerate) $\widetilde{\chi}_1^\pm/\widetilde{\chi}_2^0$ mass and the $\widetilde{\chi}_1^0$ mass. An interesting feature of this model is the possibility to reconstruct an edge in the invariant mass distribution of two leptons when they originate from the $\widetilde{\chi}_2^0$ decay via $\widetilde{\chi}_2^0 \to \ell\widetilde{\ell} \to \ell^+\ell^-\widetilde{\chi}_1^0$.

With the given sparticle masses in this example scenario, we expect an edge at 70 GeV. This signature is investigated in the opposite-sign dilepton channel. A signal is expected only for same-flavor events, while the main background, $\mathrm{t\bar{t}}$ production, also contributes (almost equally) to the different-flavor final state. The $\widetilde{\chi}_2^0$ can be produced either directly or in the decay of the third-generation sparticles.

It is remarkable that in NM1, the top squark almost never decays to the top quark (t) and the LSP ($\widetilde{\chi}_1^0$) – a typical signature that is usually searched for in simplified model approaches – but rather to a combination of $\mathrm{t}\widetilde{\chi}_2^0$, $\mathrm{t}\widetilde{\chi}_3^0$, $\mathrm{t}\widetilde{\chi}_4^0$, $\mathrm{b}\widetilde{\chi}_1^+$, and $\mathrm{b}\widetilde{\chi}_2^+$. Due to the large variety of possible final states in the top squark decay, the search results of different analyses would need to be combined in order to reach discovery sensitivity. The same is true for bottom squark searches. A typical signature to search for is the all-hadronic final state containing only two b-tagged jets and missing energy from the LSP. This channel, $\widetilde{\mathrm{b}}_1 \to \mathrm{b}\widetilde{\chi}_1^0$, constitutes only 1.5% of all possible decays, and in at least half of the possible bottom squark decays a lepton will appear, especially in the main decay chains which involve a chargino and a top quark.

The second model, called NM2, differs from NM1 mainly in the slepton masses, which are much higher than in NM1, leading to large differences in the possible sparticle decays. Here, the $\widetilde{\chi}_2^0$ decays with a large branching fraction to $\mathrm{Z}\widetilde{\chi}_1^0$ and $\mathrm{H}\widetilde{\chi}_1^0$, while the $\widetilde{\chi}_1^\pm$ decays to $\mathrm{W}\widetilde{\chi}_1^0$. If this model would be realized in nature, the search for $\widetilde{\chi}_1^\pm\widetilde{\chi}_2^0$ production should be successful in the WH and WZ channels. We test the WH channel for the leptonic decay of the W boson

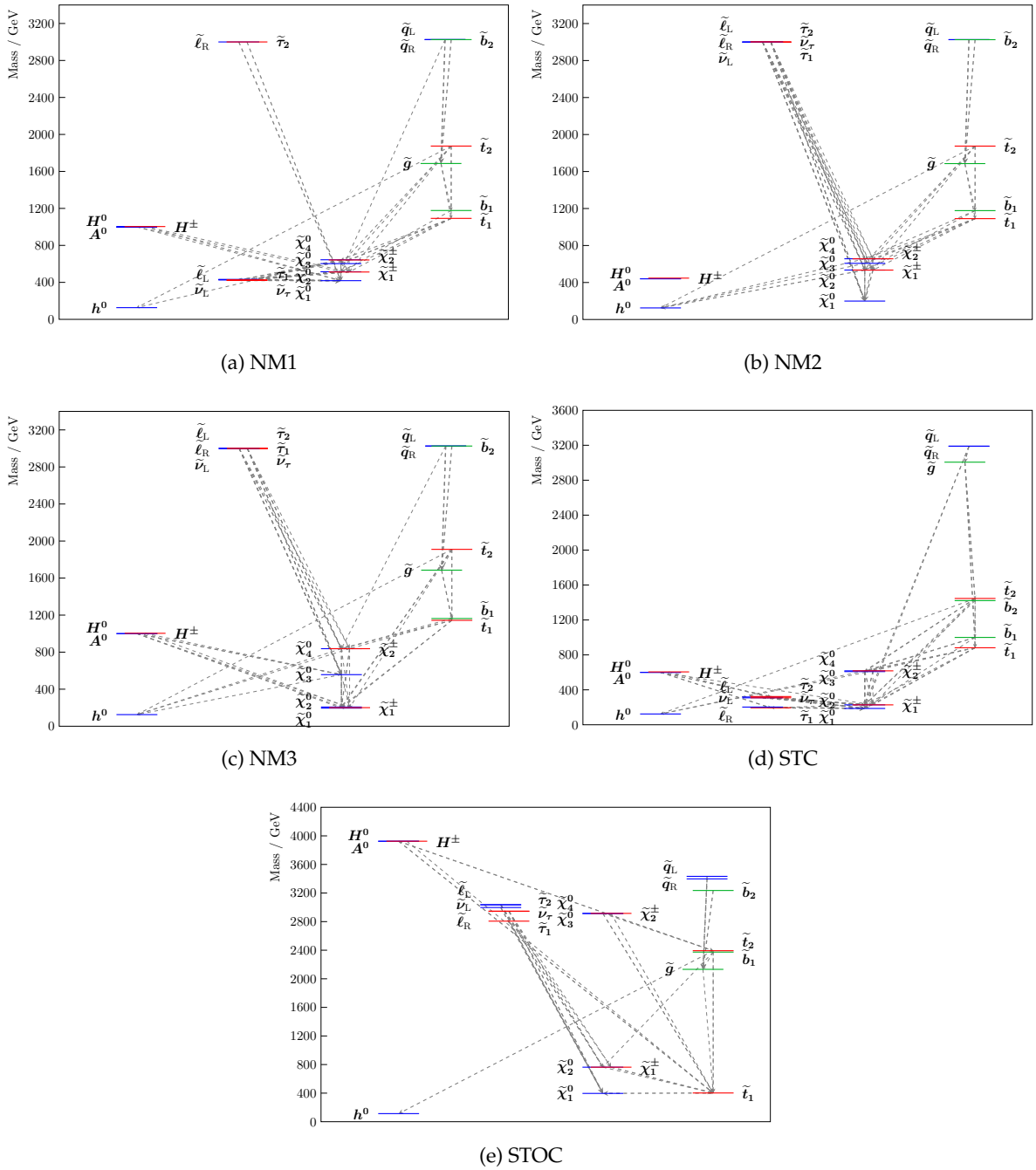

(a) NM1

(b) NM2

(c) NM3

(d) STC

(e) STOC

Figure 2: Masses of the SUSY particles in five full-spectrum SUSY models in this document and their decay lines, which are drawn for branching fractions above 5%. Shown are (a) NM1, (b) NM2, (c) NM3, (d) STC, and (e) STOC.

and the Higgs decaying to a $\mathrm{b\bar{b}}$ pair, while the WZ channel is investigated in the multilepton final state. The gluino and the third-generation squark production and decay are very similar to NM1.

In the third natural model, called NM3, most parameters are similar to the previously discussed model, NM2, with one key difference: The LSP is higgsino-like, accompanied by $\widetilde{\chi}_1^{\pm}$ and $\widetilde{\chi}_2^0$, differing in mass by only a few GeV. The different spectrum of electroweakly interacting particles leads to completely different decay chains. It will be challenging to differentiate the top and bottom squarks from each other, as the top squark mainly decays to a top quark and $\widetilde{\chi}_1^0$ or $\widetilde{\chi}_2^0$, while the bottom squark mainly decays to a top quark and $\widetilde{\chi}_1^{\pm}$, with the latter decaying to $\widetilde{\chi}_1^0$ and either a soft jet, or a soft lepton and neutrino, none of which will be easily detected. Therefore, it will be difficult to distinguish these signatures from each other, but an excess hinting for third-generation squarks will be visible for this model. In addition, the large mass difference between the third-generation squarks and the higgsinos leads to striking signatures in their dominant decay modes as discussed in more detail in Section 7.

4.2 Stau coannihilation model (STC)

Next, we discuss a model that lies in the parameter space which gained the highest likelihood in fits to all pre-LHC experimental data within the constrained MSSM (CMSSM) [29]. These fits preferred scenarios with a small mass difference of about 10 GeV between the $\widetilde{\tau}$-NLSP and the $\widetilde{\chi}_1^0$ as LSP. Within the context of the CMSSM, this region is ruled out by LHC searches based on the strongly interacting sector, which in constrained models is coupled to the electroweak sector by mass unification at the grand unified theory scale. Without the restriction of mass unification, the part of the spectrum which is of interest to electroweak and flavor precision observables and dark matter, i.e., which is decisive for the fit outcome, is not in conflict with LHC results. This applies in particular to the $\widetilde{\tau}_1$ with a small mass difference to the LSP, which is essential to allow efficient (co-)annihilation of dark matter to lower the predicted relic density to its observed value. It is further worth noting that the current limits of ewkino production are much weaker if the $\widetilde{\tau}$ is not mass-degenerate with the $\widetilde{\mathrm{e}}$ and $\widetilde{\mu}$, and has a small mass difference to the LSP [19].

In the stau coannihilation (STC) model studied here, all of the sleptons and sneutrinos are light, and the $\widetilde{\tau}_1$ and $\widetilde{\chi}_1^0$ masses are nearly degenerate, with $m_{\widetilde{\tau}_1} = 194\,\mathrm{GeV}$ and $m_{\widetilde{\chi}_1^0} = 187\,\mathrm{GeV}$. The gluino is heavy ($m_{\widetilde{\mathrm{g}}} \approx 3\,\mathrm{TeV}$), suppressing its production; this is the only benchmark model in which the gluino pair production cross section is effectively negligible. However, the $\widetilde{\mathrm{t}}_1$ and $\widetilde{\mathrm{b}}_1$ are relatively light, with $m_{\widetilde{\mathrm{t}}_1} = 882\,\mathrm{GeV}$ and $m_{\widetilde{\mathrm{b}}_1} = 1.00\,\mathrm{TeV}$. These masses lead to significant direct pair-production cross sections of 19 fb for $\widetilde{\mathrm{t}}_1\widetilde{\mathrm{t}}_1^*$ and 8.3 fb for $\widetilde{\mathrm{b}}_1\widetilde{\mathrm{b}}_1^*$. (Antiparticles of SUSY partners are denoted here with an asterisk.) The decay $\widetilde{\mathrm{b}}_1 \to \mathrm{b}\widetilde{\chi}_1^0$ has a large branching fraction ($\approx 70\%$) and provides a key signature in an all-hadronic search. As a consequence of $\widetilde{\mathrm{t}}_1$ decays to the low-mass electroweak sector, the single-lepton $\widetilde{\mathrm{t}}_1$ search and the trilepton + b-tag search both provide good sensitivity.

4.3 Stop coannihilation model (STOC)

We also consider a stop coannihilation (STOC) model [30, 31] formulated in the CMSSM parameter space. In this model, the top squark mass (402 GeV) is much lower than that in other benchmark models and the direct top squark pair production cross section is enormous (≈ 2100 fb). The top squark is also nearly mass-degenerate with the $\widetilde{\chi}_1^0$, which is bino-like. As a consequence, the top squark decays are effectively invisible, because they proceed via the loop process $\widetilde{\mathrm{t}}_1 \to \mathrm{c}\widetilde{\chi}_1^0$, in which the daughter charm jet is extremely soft due to the small mass

splitting between $\widetilde{t}_1$ and $\widetilde{\chi}_1^0$. Nevertheless, if the $\widetilde{t}_1\widetilde{t}_1^*$ system is boosted against a hard jet from initial-state radiation, the process is experimentally accessible in the monojet + E_T^{miss} like signature, as discussed in more detail in Section 10.

In the STOC model, the gluino is the second lightest strongly interacting particle, with $m_{\widetilde{g}} = 2.13$ TeV. The gluino pair production cross section is ≈ 0.5 fb, about one-tenth of that in NM1–NM3. The squark-gluino cross section is comparable (≈ 0.3 fb), and squarks dominantly decay to light quarks and the gluino. The gluino is light enough to be visible, but the discovery channel differs from the other models, as the top squark is essentially invisible due to its decay to the only slightly lighter $\widetilde{\chi}_1^0$. Therefore, the expected final state from gluino-gluino and squark-gluino production includes two top quarks and large missing transverse momentum, which are accessible in the all-hadronic H_T-H_T^{miss} analysis as well as in the single-lepton analysis nominally targeted for stop pair production in other models. Discoveries of new physics in the monojet signature and $t\bar{t}$ + E_T^{miss} signature combined with absence of new physics in the $b\bar{b}$ + E_T^{miss} signature would provide strong indication of this scenario.

4.4 Analysis overview

Nine different analyses are performed on these SUSY models to see what we will learn in the LHC Run 2 and Run 3 and in the HL-LHC.

Several analyses are designed to search for colored sparticles in the all-hadronic final state, either inclusive, searching for a large amount of hadronic energy and missing transverse energy, referred to H_T-H_T^{miss}, or exploiting special kinematic variables, as in the M_{T2} analysis, based on existing 8 TeV analyses [18, 32, 33] with adjusted selection requirements. Other analyses target the discovery of specific sparticles, like $\widetilde{b}_1$ or $\widetilde{t}_1$ in direct production. For these searches, we also use tightened requirements from 8 TeV analyses, given in Ref. [34] for the $\widetilde{b}_1$ search and in Ref. [35] for the $\widetilde{t}_1$ search.

A special case to search for is the stop coannihilation model, where $\widetilde{t}_1$ and $\widetilde{\chi}_1^0$ are almost mass-degenerate, causing all final state particles to be very soft, such that they can only be triggered by a single jet from initial-state radiation. A search in the monojet signature has also been performed on 8 TeV data [36], and a similar search is performed here too with tighter selections.

We also search for direct production of ewkinos, mainly $\widetilde{\chi}_1^\pm\widetilde{\chi}_2^0$ production. Here we investigate two decay modes, where in both cases the $\widetilde{\chi}_1^\pm$ decays to a W boson and a $\widetilde{\chi}_1^0$, while the $\widetilde{\chi}_2^0$ decays either to a Z boson and a $\widetilde{\chi}_1^0$ or a Higgs boson and a $\widetilde{\chi}_1^0$. As W and Z can decay leptonically, we investigate here a three-lepton final state, while for the WH search the Higgs decay to two b-quarks is exploited while requiring one lepton from the W decay, similar to the analyses presented in Ref. [19].

Table 1 briefly summarizes the results of all the studies presented in Sections 6–13. Here we identify the expected sensitivity reach for each analysis and the models it was applied to. The ranges were chosen as indication of "low sensitivity" (grey), "evidence" (light blue), and "discovery" (dark orange). The main message we intend to convey here is the richness of physics that can be studied with the HL-LHC if new physics is discovered by the end of Run 3 data taking.

Table 1: Overview of the SUSY analyses and their application to the full-spectrum benchmark models.

Analysis	Luminosity (fb^{-1})	Model				
		NM1	NM2	NM3	STC	STOC
all-hadronic (H_T-H_T^{miss}) search	300					
	3000					
all-hadronic (M_{T2}) search	300					
	3000					
all-hadronic $\widetilde{b}_1$ search	300					
	3000					
1-lepton $\widetilde{t}_1$ search	300					
	3000					
monojet $\widetilde{t}_1$ search	300					
	3000					
$m_{\ell^+\ell^-}$ kinematic edge	300					
	3000					
multilepton + b-tag search	300					
	3000					
multilepton search	300					
	3000					
ewkino WH search	300					
	3000					

$< 3\sigma$ | $3 - 5\sigma$ | $> 5\sigma$

5 Analysis strategy

5.1 Monte Carlo simulation

We study two main detector configurations: in order to determine the discovery sensitivity with $300\,\mathrm{fb}^{-1}$, we use the Phase I detector with 50 pileup interactions [37–39], while for the HL-LHC we exploit a Phase II baseline detector configuration with a pileup of 140. In addition, we also investigate the possibility to further run with an aged Phase I detector beyond $300\,\mathrm{fb}^{-1}$, when significant radiation damage is expected for the tracker and the endcap calorimeters.

Monte Carlo simulation samples have been produced with these configurations based on a preliminary GEANT 4 detector simulation, from which the object efficiencies and resolutions have been determined and implemented in the DELPHES 3.0.10 fast simulation program [26], which is used for signal and background production. A further tuning of the full detector simulation is ongoing. DELPHES is able to include pileup interactions from inelastic proton-proton interactions simulated with PYTHIA 6.4 [25]. These events are randomly distributed along the beam axis (also called z-axis) according to a Gaussian distribution with a width of 0.053 m. If the z-position of a pileup vertex is less than the 0.1 mm from the primary vertex (corresponding to the resolution), the pileup interaction is not separated from the additional vertices, and all particles from both the pileup and primary interactions are included in the object reconstruction. For pileup interactions with a larger z-vertex difference to the primary

vertex, the subtraction of charged pileup particles within the tracker volume is applied with an efficiency of unity. The FastJet area method [40] is applied to correct measurements of jets and energy in the calorimeters for the contribution from neutral pileup particles and charged pileup particles outside the tracker acceptance.

About 10 to 100 million events per background process are produced with MADGRAPH 5 [23, 24], including up to four extra partons from initial and final state radiation, matched to PYTHIA 6.4 for fragmentation and hadronization. The background cross section is normalized to the next-to-leading-order (NLO) cross section, which is based on the work in preparation for the Snowmass summer study 2013 and discussed in more detail in Refs. [41–43].

5.2 Evaluation of systematic uncertainties

All presented studies are based on 8 TeV analyses, where the systematic uncertainties have been evaluated based on the various background estimation methods. We assume that the backgrounds will be estimated in a similar way for the 14 TeV analyses in the future, while in this paper we use the Monte-Carlo prediction only. Therefore, we use the systematic uncertainties of the 8 TeV analyses as starting point, and scale them on a case-by-case basis depending on their origin and predicted development of this origin:

- If the selection requirements of the 14 TeV analysis have been tightened such that the background yield in the signal region is comparable to the one in the 8 TeV analysis, we quote a typical uncertainty from the 8 TeV search. This is the case for both all-hadronic analyses with H_{T}-$H_{\mathrm{T}}^{\mathrm{miss}}$ and M_{T2} variables.
- If the uncertainty quoted for the 8 TeV analysis is caused by a systematic effect that is likely not to change, we keep the same systematic uncertainty for the 14 TeV analysis as well. This applies to the trilepton search as well as to the bottom and top squark searches.
- If the systematic uncertainty for the corresponding 8 TeV analysis is limited predominantly by the statistics in the estimation method, which is expected to improve, we assume a reduction in the systematic uncertainty by a factor of 2. This is the case in the ewkino WH analysis.
- For an analysis with high statistics we break down the sources of the uncertainty. Those originating from systematic nature stay the same, while those from the statistics nature, e.g. control sample statistics are scaled according to the predicted statistics. This procedure is applied in the monojet stop search.

5.3 Significance calculation

For all models, we determine the discovery significance. For this, we determine the significance in one-sided Gaussian standard deviations for a counting experiment in a hypothesis test between background only and signal + background including an uncertainty on the background estimate. The problem is treated in a fully frequentist fashion by interpreting the relative background uncertainty as being due to a sideband observation that is also Poisson distributed with only background. Finally, one considers the test as a ratio of Poisson means where an interval is well known based on the conditioning on the total number of events and the binomial distribution. For counting experiments with a single bin this is done with Roostats [44] using the Binominal significance Z_{Bi} [45–47]. For analyses with multiple signal regions, we use the Roostats tool developed by the LHC Higgs Combination Group [48].

6 Inclusive search in the all-hadronic final state with H_T and H_T^{miss} variables

This search targets R-parity conserving SUSY scenarios, where heavy colored particles are produced. The signature is based on the assumption that long decay chains lead to signatures with multiple jets and large missing transverse momentum. Several all-hadronic (lepton-vetoed) searches were performed by the CMS Collaboration using data taken at 7 and 8 TeV both with and without b-tagging requirements [32, 33, 49–52]. The search targets a signal that leads to a large amount of hadronic energy $H_T = \sum_{jets} p_T$ for jets with $p_T > 50\,GeV$ and $|\eta| < 2.5$ in conjunction with missing hadronic transverse energy which is defined as $H_T^{miss} = |-\sum_{jets} \vec{p}_T|$ for jets with $p_T > 30\,GeV$ and $|\eta| < 5$. This search investigates the discovery sensitivity for heavy colored particle signals in the STC and STOC models with multiple jets, some of which are b-tagged (medium working point), and high H_T and H_T^{miss}.

The SM background to this SUSY search arises mainly from three processes: $Z(\nu\bar{\nu})$ + jets events, and $W(\ell\nu)$ + jets events from W or $t\bar{t}$ + jets, where at least one W boson decays leptonically (ℓ = e, μ, or τ). The $W(\ell\nu)$ + jets events pass the search selection when the e/μ escapes detection or when a τ decays hadronically. QCD multijet events also contribute to the background when jet energy mismeasurements or leptonic decays of heavy-flavor hadrons inside jets lead to H_T^{miss}; however, the QCD background generally becomes negligible at high H_T^{miss}, so it is not considered in this study.

The analysis starts with a set of events that pass the following baseline selection criteria motivated by the 8 TeV analysis [32]. We require at least three jets with $p_T > 50\,GeV$ and $|\eta| < 2.5$, $H_T > 1000\,GeV$, and $H_T^{miss} > 500\,GeV$. In order to suppress QCD background, events are required to satisfy $|\Delta\phi(j_n, \vec{H}_T^{miss})| > 0.5$ for $n = 1, 2$ and $|\Delta\phi(j_3, \vec{H}_T^{miss})| > 0.3$, where $\Delta\phi$ is the azimuthal angle difference between the jet axis j_n and the $\vec{H}_T^{miss}$ direction. We veto events with isolated muons satisfying $p_T > 10\,GeV$ and $|\eta| < 2.4$ or electrons with $p_T > 10\,GeV$ and $|\eta| < 2.5$ which suppress the $t\bar{t}$ and $W(\ell\nu)$ + jets background. We also veto events with isolated photons with $p_T > 30\,GeV$.

The most recent searches by CMS with this search strategy [32, 33] divide these events further into several exclusive search regions defined according to the jet multiplicity (N_{jets}), H_T, and H_T^{miss} or b-tag multiplicity ($N_{b\text{-}tags}$), H_T, and H_T^{miss}. In this projection study, for simplicity, we use only one search region defined with $H_T > 2500\,GeV$, $N_{b\text{-}tags} \geq 2$, and $H_T^{miss} > 1300\,GeV$. The distributions of $N_{b\text{-}tags}$, H_T^{miss}, and H_T are shown in Fig. 3 and Fig. 4(a), and event yields for the SM backgrounds and STC and STOC signals are shown in Table 2. We assume 30% uncertainty on the background prediction, based on the typical background uncertainty in the recent CMS analyses [32, 33]. With $3000\,fb^{-1}$ of data, we will be able to have $> 5\sigma$ observation of the STOC model signal or 3–5σ evidence of the STC model signal as shown in Fig. 4(b).

In addition to the 5σ observation of the SUSY signal, the b-tag and H_T distributions in Fig. 3(a) and Fig. 4(a) may be used to extract features of the SUSY spectrum, e.g., the fact that the SUSY signal is expected in the STOC model to predominantly populate $N_{b\text{-}tags} = 2$ rather than $N_{b\text{-}tags} \geq 3$ supports a hypothesis of $\tilde{g} \to t\tilde{t}_1$, where the top squark $\tilde{t}_1$ is degenerate with $\tilde{\chi}_1^0$. The H_T distribution shown in Fig. 4(a) itself would furthermore indicate the presence of gluino-squark production, with high mass first two generation squarks of about 3.4 TeV. Further study of kinematic distributions may shed more light on the nature of the new physics seen in this scenario, but are outside the scope of this document.

Table 2: All-hadronic inclusive search with H_T and H_T^{miss}: Background and signal event yields corresponding to 3000 fb^{-1}. The vector boson denoted by "V" refers to W, Z, and γ.

Selection	$t\bar{t}$	V + jets	VV	Single top	Other	Total SM	STC	STOC
$N_{jets} \geq 3$	18600	505000	11600	661	3910	540000	7070	1380
$H_T > 2500$ GeV	396	2100	220	9.5	61	2790	208	388
$N_{b\text{-tags}} \geq 2$	132	35	5.3	2.4	12	186	62	104
$H_T^{miss} > 1300$ GeV	1.6	2.4	0.4	0.1	0.4	4.9	17	49

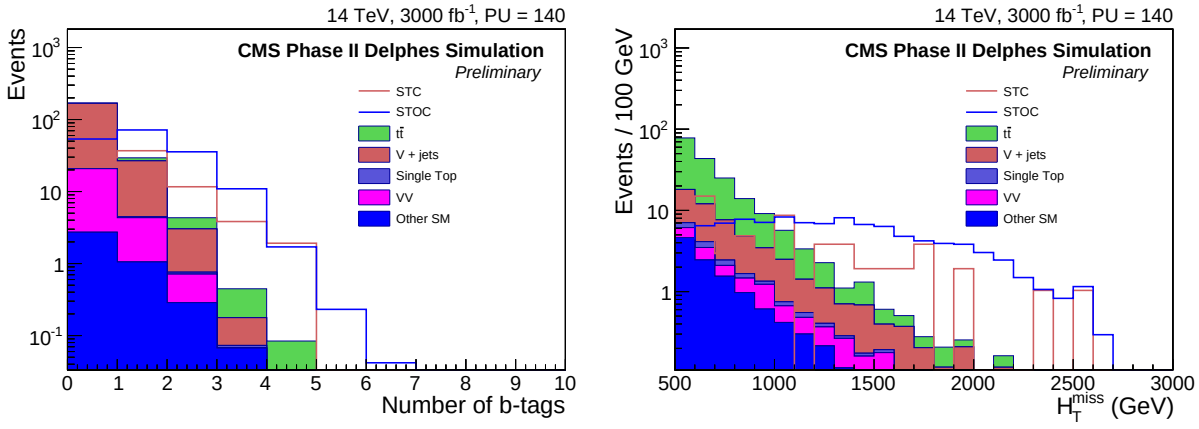

(a) (b)

Figure 3: All-hadronic inclusive search with H_T and H_T^{miss}: (a) the b-tag multiplicity distribution for events passing all the search selections except for the b-tag multiplicity requirement, and (b) H_T^{miss} distribution for events passing all the search selections except for the H_T^{miss} requirement. The contributions of the SM backgrounds are shown as stacked histograms, as they are elsewhere in this document. The SUSY signal contributions from different models are shown overlaid.

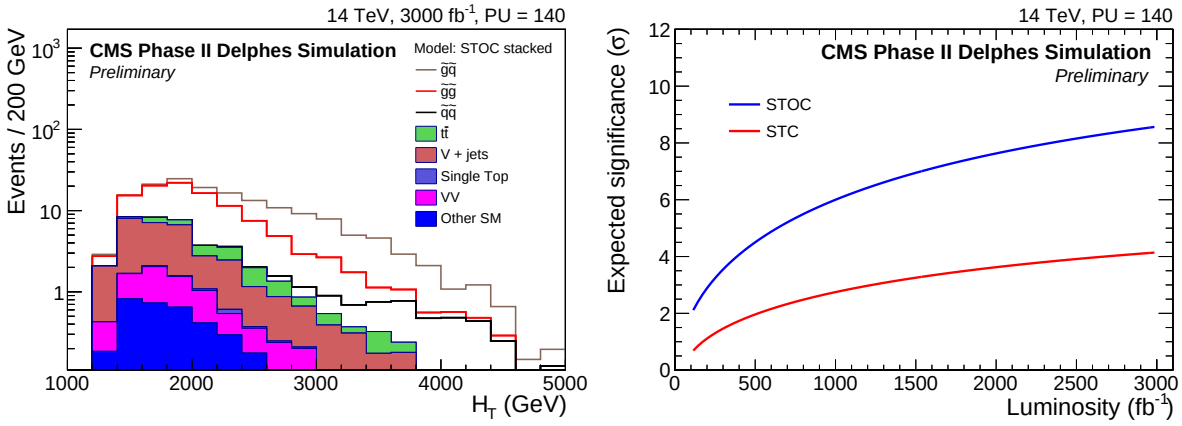

(a) (b)

Figure 4: All-hadronic inclusive search with H_T and H_T^{miss}: (a) the H_T distribution for the background and STOC signal events in the search region. In this figure, the signal contributions are shown stacked, as they are from different sparticle production processes in a single model, STOC. (b) Discovery significance as a function of the integrated luminosity.

7 Inclusive search in the all-hadronic final state with the M_{T2} variable

This analysis targets the natural models NM1, NM2, and NM3 described in Section 4, where the discovery of gluino pair production is expected to lead to two decay chains each including an unobserved LSP. The so-called "stransverse" mass M_{T2} [53, 54] is designed for such a signature, and its endpoint would yield the mass of the two pair-produced sparticles, here the gluino mass.

This analysis is based on the CMS M_{T2} analysis performed at 7 and 8 TeV [18, 55], an all-hadronic selection that uses M_{T2} as a discriminating variable instead of H_T^{miss}. Many features of this analysis, including the M_{T2} calculation and the hemisphere calculation, are identical or similar to those used in the 7 and 8 TeV analyses [18, 55].

The natural models feature gluino decays through top and bottom squarks, and thus tend to have large numbers of b-tagged jets and high jet multiplicity. For jet counting and b-tagging, we use jets with $p_T > 40\,GeV$ and $|\eta| < 2.4$. H_T is defined here as the scalar sum of the p_T of jets with $p_T > 50\,GeV$ and $|\eta| < 3.0$. M_{T2} is reconstructed using jets with $p_T > 30\,GeV$ and $|\eta| < 2.4$.

To suppress backgrounds with real missing transverse energy from $W \to \ell\nu$ decays, we veto events with electrons and muons with $p_T > 10\,GeV$ and $|\eta| < 2.4$ that have a relative isolation smaller than 0.2. To suppress QCD background, we require $\Delta\phi_{min}(\text{jets}, E_T^{miss}) > 0.3$, which is computed using the four leading jets with $p_T > 40\,GeV$ and $|\eta| < 2.4$. The missing transverse energy, E_T^{miss}, is defined as the absolute value of the negative vector sum p_T of all reconstructed objects in the detector. After the tight requirements on b-tagging and M_{T2} given below, we assume that QCD background is negligible. We require $|\vec{E}_T^{miss} - \vec{H}_T^{miss}| < 175\,GeV$ in order to suppress events with large upstream transverse momentum.

A tight search region is defined by requiring the number of jets ≥ 8, at least three medium b-tags, $H_T > 1500\,GeV$, and M_{T2} requirements ranging from 500 to 800 GeV, as function of luminosity. After this selection, the dominant production mode is gluino-gluino, although there is a non-negligible contribution from squark-gluino production.

Table 3 shows yields for signal and background in $3000\,fb^{-1}$. The resulting discovery potential depends on the systematic uncertainty of the background estimate. As comparable search regions (with a three b-tag requirement and only a handful of background events) in the 8 TeV M_{T2} analysis have relatively large systematic uncertainties of roughly 45%, mainly due to statistical limitation in the regions used for background estimation, we expect a similar uncertainty with the tightened selection requirements as discussed above.

Figure 5 shows distributions of the number of b-tagged jets for the three investigated signal models and the M_{T2} variable after the application of all selection criteria except the M_{T2} requirement. The evolution of the discovery potential as a function of luminosity is shown in Fig. 6. The discovery sensitivity to the NM1 model is lower compared to the sensitivities to NM2 and NM3. This effect is a consequence of the lower efficiency of the signal selection due to the lepton veto by a factor of about 2. This difference in the lepton veto efficiency is due to different branching fractions of $\widetilde{\chi}_1^{\pm}$ and $\widetilde{\chi}_2^0$ (originating from gluino decays) into the final states including leptons, which is much higher for NM1 than for NM2 and NM3. The discovery sensitivity for NM3 is higher than that for NM2 because of the harder M_{T2} spectrum of the signal for NM3 than for NM2 as shown in Fig. 5(b). This is due to the lower $\widetilde{\chi}_1^{\pm}$ and $\widetilde{\chi}_2^0$ masses in NM3 than in NM2, which makes the $\widetilde{t}_1$ and $\widetilde{b}_1$ decays more energetic leading to a harder M_{T2}

Table 3: All-hadronic inclusive search with M_{T2}: Estimated event yields for signal samples and SM background processes corresponding to 3000 fb^{-1}. Requirements on $|\vec{E}_T^{miss} - \vec{H}_T^{miss}|$, $\Delta\phi_{min}$, and lepton vetoes are applied for all rows. The "other" category consists of the multiboson samples.

Selection	$t\bar{t}$	V + jets	Single top	VV	Other	Total SM	NM1	NM2	NM3
$N_{jets} \geq 8$	6110000	3120000	333000	117000	110000	9790000	2240	7770	4720
$H_T > 2000$	79700	97100	3570	3630	2150	186000	751	3090	2080
$N_{b\text{-tags}} \geq 3$	13500	1570	500	66	430	16100	361	1730	973
$M_{T2} > 500$ GeV	12.5	1.0	0.6	0.1	1.6	16	98	277	408
$M_{T2} > 600$ GeV	5.1	0.8	0.3	0.1	1.3	7.5	63	162	317
$M_{T2} > 800$ GeV	1.2	0.3	0.1	0.0	0.6	2.3	28	50	136

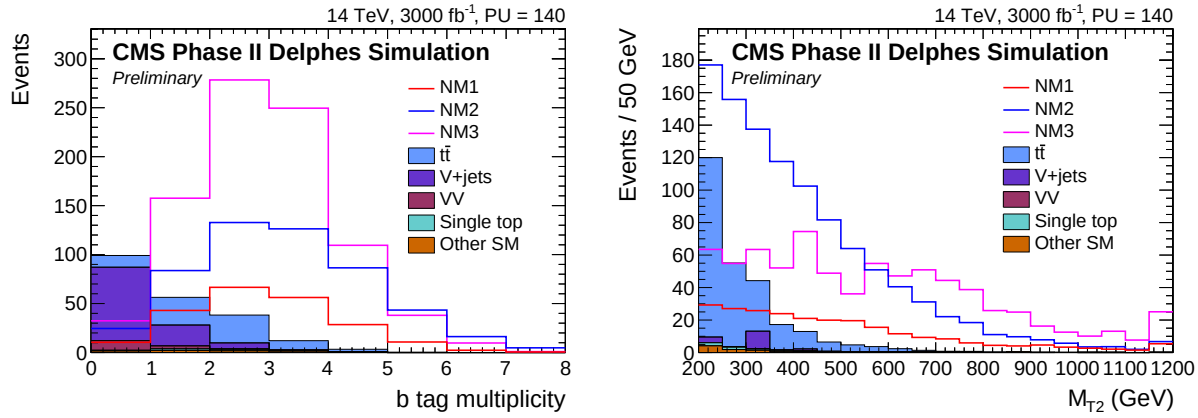

(a) (b)

Figure 5: All-hadronic inclusive search with M_{T2}: (a) The distribution of the number of jets with the medium b-tag requirement, using the signal selection given in the text including a requirement of $M_{T2} > 500$ GeV, and (b) the distribution of M_{T2} after the full selection (including ≥ 3 b-tags) except the M_{T2} requirement itself.

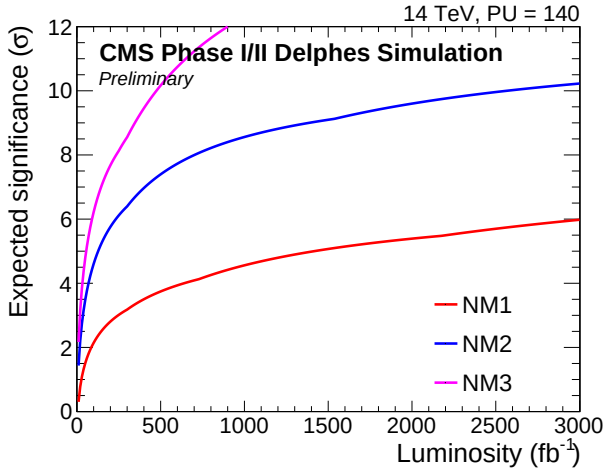

Figure 6: All-hadronic inclusive search with M_{T2}: Significance for the models NM1, NM2, and NM3. The model NM3 has the highest discovery significance.

spectrum.

8 Search for $\widetilde{\mathrm{b}}$ pair production in the all-hadronic final state

In this section, we investigate the discovery potential for third-generation squarks in the final state with two b-jets and missing energy. If the $\widetilde{\chi}_1^{\pm}$ and the $\widetilde{\chi}_1^0$ are not degenerate, the contribution of the top squark to this final state will be small and distinguishing bottom and top squarks might be possible.

Of particular interest for this search is the decay $\widetilde{\mathrm{b}}_1 \to \mathrm{b}\widetilde{\chi}_1^0$, which is the dominant decay mode of bottom squark in the stau coannihilation (STC) model scenario with branching fraction of 68%. Assuming that the bottom squarks are pair-produced, a final state containing exactly two b-quarks and two neutralinos is expected for over 50% of the signal events. Since for all other SUSY models considered in this study the bottom and top squarks rarely decay into such a final state with only two b-jets and $E_{\mathrm{T}}^{\mathrm{miss}}$, third-generation squarks would not be discovered in this specific channel. In fact, the lack of sensitivity to the other four models indicates that this final state can hardly be contaminated by decays of other colored sparticles, e.g., gluinos, even if they are not too heavy. On the other hand, a lack of an excess in this final state can be used to exclude a part of the SUSY phase space, when excesses are observed in other SUSY searches.

The search regions are based on the search for direct sbottom production using the 8 TeV data described in Ref. [34]. The events are required to contain exactly two central jets with $|\eta| < 2.4$ and $p_{\mathrm{T}} > 300$ and 200 GeV, respectively. Both leading jets are required to be identified as originating from a bottom quark. Events with a third jet with $p_{\mathrm{T}} > 70$ GeV or a lepton (e or μ) with $p_{\mathrm{T}} > 10$ GeV and $|\eta| < 2.5$ are rejected. We require $H_{\mathrm{T}} > 750$ GeV, where H_{T} is the scalar sum of p_{T} of the two leading jets in the events. $E_{\mathrm{T}}^{\mathrm{miss}}$ is required to be above 450 GeV. In order to reject background from dijet QCD processes, we impose a cut on the azimuthal angle between the two leading jets of $\Delta\phi(j_1, j_2) < 2.5$. We expect QCD dijet events to be back to back, in contrast to the b-jets in the signal process. To suppress SM processes like $\mathrm{t\bar{t}}$ and $\mathrm{W}(\ell\nu)$ + jets, we require the minimum invariant transverse mass of one of the two b-tagged jets and the missing transverse energy, $\min(M_{\mathrm{T}}(j_{1,2}, E_{\mathrm{T}}^{\mathrm{miss}}))$ to be above 500 GeV.

Going one step further, in case of a discovery, one can use the so-called boost-corrected contransverse mass (M_{CT}) [56, 57], which is defined as

$$\begin{aligned} M_{\mathrm{CT}}^2(j_1, j_2) &= [E_{\mathrm{T}}(j_1) + E_{\mathrm{T}}(j_2)]^2 - [\vec{p}_{\mathrm{T}}(j_1) - \vec{p}_{\mathrm{T}}(j_2)]^2 \\ &= 2p_{\mathrm{T}}(j_1)p_{\mathrm{T}}(j_2)(1 + \cos\Delta\phi(j_1, j_2)) \end{aligned}$$

in order to determine the mass of the new particle. This variable is useful for extracting information from events in which two heavy particles decay into a jet and missing energy, as is the case for the pair of bottom squark decays considered here. The $M_{\mathrm{CT}}(j_1, j_2)$ distribution is characterized by an endpoint defined by $m_{\widetilde{\mathrm{b}}_1}$ and $m_{\widetilde{\chi}_1^0}$, which for the topology in question is at $(m_{\widetilde{\mathrm{b}}_1}^2 - m_{\widetilde{\chi}_1^0}^2)/m_{\widetilde{\mathrm{b}}_1}$. We therefore expect to observe a kinematic edge in the $M_{\mathrm{CT}}(j_1, j_2)$ distribution, as seen in Fig. 7.

The number of events for different SM processes and inclusive signal samples after each selection step, and in four different search bins, defined by different $\min(M_{\mathrm{T}}(j_{1,2}, E_{\mathrm{T}}^{\mathrm{miss}}))$ requirements, are shown in Table 4. The event yields in the table are based on the respective cross sections at 14 TeV, normalized to a luminosity of 3000 fb^{-1}.

Additionally we test the purity of this analysis selection with respect to the process of interest, $\widetilde{\mathrm{b}}_1 \to \mathrm{b}\widetilde{\chi}_1^0$. Table 5 shows the expected signal yields of the inclusive sample after all analysis selection criteria are applied. We find that more than 87% of the selected signal events in the different search regions are $\widetilde{\mathrm{b}}_1 \to \mathrm{b}\widetilde{\chi}_1^0$ events. The other bottom squark decay modes and all the

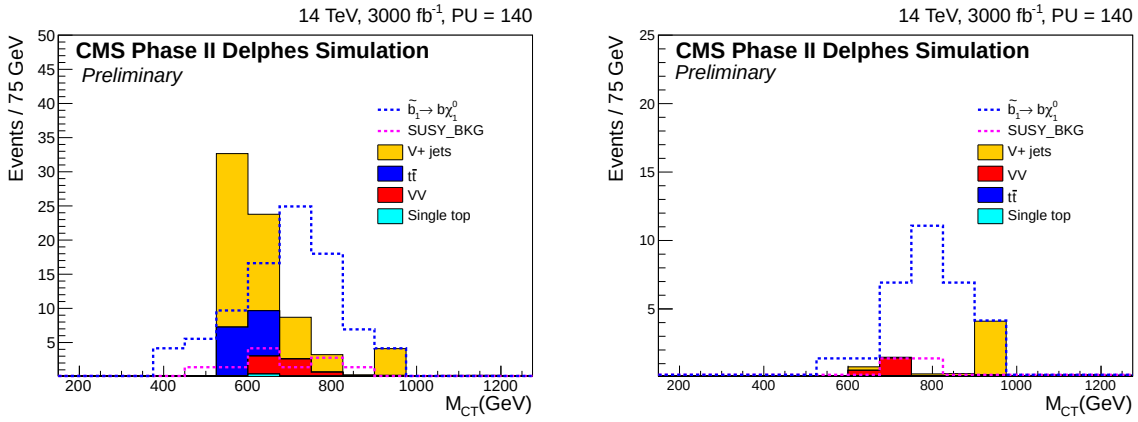

(a) (b)

Figure 7: Search for bottom squarks: Comparison of the M_{CT} distribution for signal and background from SM and other SUSY processes. The SUSY processes from the STC model are considered in these figures. All selection requirements are applied. The two figures show the signal region for (a) $M_T > 750\,\text{GeV}$ and (b) $M_T > 950\,\text{GeV}$, respectively. The endpoint for all signal regions is located at the same position. The background distributions are stacked, while the signal and other SUSY contributions are overlaid.

Table 4: Search for bottom squarks: The event yields for the STC signal sample and several SM processes with $3000\,\text{fb}^{-1}$ at 14 TeV with 140 pileup interactions. The variable M_T is the minimum invariant transverse mass of one of the two b-tagged jets and the missing transverse energy. The pre-selection refers to events passing all the requirements except the selection on H_T, E_T^{miss}, and M_T.

Selection	Diboson	$t\bar{t}$	W/Z + jets	single top	Total SM	STC
Pre-selection	1800	38700	157000	10800	208000	360
$H_T > 750\,\text{GeV}$	999	20400	65000	5280	91700	249
$E_T^{miss} > 450\,\text{GeV}$	10	262	119	12	405	152
$M_T > 500\,\text{GeV}$	7	33	81	0	124	144
$M_T > 750\,\text{GeV}$	6	13	53	0	72	102
$M_T > 850\,\text{GeV}$	4	0	24	0	28	70
$M_T > 950\,\text{GeV}$	2	0	5	0	7	34

events that originate from top squark decays are treated as SUSY background in this analysis. We are therefore able to distinguish bottom from top squarks if the non-degeneracy of chargino and neutralino is confirmed independently.

In case of discovery in this channel we would be able to measure the third-generation squark production cross section multiplied by the branching fraction, $\mathcal{B}(\tilde{b}_1 \to b\tilde{\chi}_1^0)$. Depending on the number of signal events in each search bin, the uncertainty on the cross section times branching fraction ranges from 18–30% for the different search bins, assuming 10% uncertainty on the predicted background and signal efficiency, and 3% uncertainty on the luminosity. The expected sensitivity as a function of integrated luminosity are shown in Fig. 8. An excess of 3σ is expected in the third search bin with $M_T > 850\,\text{GeV}$ and $300\,\text{fb}^{-1}$ of data, and discovery sensitivity is expected with $1000\,\text{fb}^{-1}$.

Table 5: Search for bottom squarks: The composition of the inclusive signal sample after applying all selection requirements in the search region. The variable M_T is the minimum invariant transverse mass of one of the two b-tagged jets and the missing transverse energy.

Selection	Total SM	STC	all $\tilde{t}_1$ decays	$\tilde{b}_1 \to b\tilde{\chi}^0_{2,3,4}$	$\tilde{b}_1 \to b\tilde{\chi}^0_1$
$M_T > 500\,\text{GeV}$	124	144	11	8	125
$M_T > 750\,\text{GeV}$	72	101	7	4	90
$M_T > 850\,\text{GeV}$	28	70	3	3	64
$M_T > 950\,\text{GeV}$	7	34	1	1	32

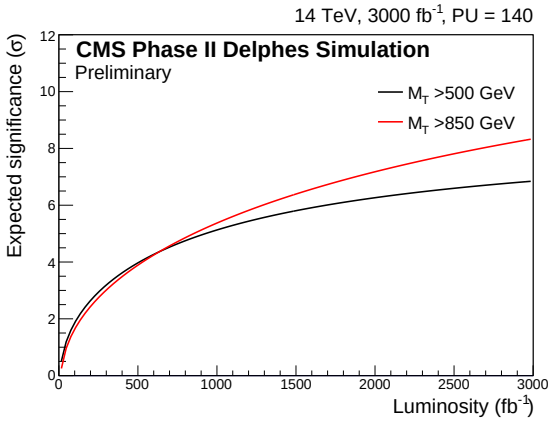

Figure 8: Search for bottom squarks: Expected sensitivity in different search bins as a function of integrated luminosity.

When looking for a new particle like the bottom squark in an exclusive decay mode, once it is confirmed that the top squark does not contaminate this final state, we might be able to gain more information about its parameters by analyzing kinematic variables like M_{CT}. In order to set an upper limit on the sparticle mass we would need to extract the endpoint for M_{CT}. Due to the contamination from SM processes or SUSY background the endpoint might be hidden or smeared. The contribution from SM processes can be estimated from MC simulation or using data driven methods, but a priori unknown SUSY background cannot be eliminated. The M_{CT} distribution is shown as an example in Fig. 7 for two different signal regions. They are consistent with the expected endpoint of 965 GeV in all four signal regions. Without further knowledge about the $\tilde{\chi}^0_1$, this endpoint can be interpreted as lower limit on the bottom squark mass. If another analysis would arrive at determining the $\tilde{\chi}^0_1$ mass, we would even be able to determine the bottom squark mass.

In turn, we could use this measured mass to calculate the cross section for this process and compare it to the cross section times branching fraction determined above from counting the events in the signal region. While the mass determination is independent of the spin of the newly discovered particle, the measured event rate that can be related to the cross section (times branching fraction) depends on the spin of the new particle. Final conclusions could only be drawn if the branching fraction could be determined in addition.

9 Search for $\widetilde{\mathrm{t}}$ pair production in the single-lepton final state

In this section, we discuss the search for direct top squark pair production. Typical 8 TeV analyses mainly consider simplified models in which two top squarks are produced, with each decaying into either $\mathrm{t}\widetilde{\chi}_1^0$ or $\mathrm{b}\widetilde{\chi}_1^{\pm}$. The models proposed here show a wide variety of top squark decay modes. As an example, in the STC model only 4% of $\widetilde{\mathrm{t}}_1\widetilde{\mathrm{t}}_1^*$ events are expected to have a decay mode $\widetilde{\mathrm{t}}_1\widetilde{\mathrm{t}}_1^* \to (\mathrm{t}\widetilde{\chi}_1^0)(\bar{\mathrm{t}}\widetilde{\chi}_1^0)$. Additionally, bottom squark pair production enters as a sizable intrinsic SUSY background when one of the bottom squarks decays to $\mathrm{b}\widetilde{\chi}_1^0$ and the other one decays to $\mathrm{t}\widetilde{\chi}_1^{\pm}$. In the natural models NM1, NM2, and NM3, gluino pair production provides the main intrinsic background with a large number of jets, b-jets, and large $E_{\mathrm{T}}^{\mathrm{miss}}$ due to the process $\widetilde{\mathrm{g}}\widetilde{\mathrm{g}} \to (\mathrm{t}\bar{\mathrm{t}}\widetilde{\chi}_1^0)(\mathrm{t}\bar{\mathrm{t}}\widetilde{\chi}_1^0)$. We therefore face two major challenges in this analysis, one being large SM background and the other one being background from other SUSY processes.

The analysis method is similar to the one in the CMS 8 TeV analysis [35], but with tighter selection requirements. We require a single isolated electron or muon with $p_{\mathrm{T}} > 30\,\mathrm{GeV}$ and $|\eta| < 2.4$. Events are vetoed if there are additional isolated leptons or tracks with $p_{\mathrm{T}} > 20\,\mathrm{GeV}$. In addition, we require at least five jets with $p_{\mathrm{T}} > 40\,\mathrm{GeV}$ and $|\eta| < 2.4$, which enhances the fraction of $\widetilde{\mathrm{t}}_1\widetilde{\mathrm{t}}_1^*$ events with respect to $\widetilde{\mathrm{b}}_1\widetilde{\mathrm{b}}_1^*$ events. One or two of these jets must satisfy a medium b-tag requirement. To further reduce the SM background, we require $E_{\mathrm{T}}^{\mathrm{miss}} > 400\,\mathrm{GeV}$.

Additionally, we introduce an angular variable $\min \Delta\phi$, the minimum azimuthal angle between the leading jet or subleading jet and the $E_{\mathrm{T}}^{\mathrm{miss}}$. For this variable we require events to have a value greater than 0.8 in order to reduce backgrounds from SM processes. Another variable that aids in reducing backgrounds is centrality, defined as the sum of the p_{T} of the lepton and jets divided by their total momentum $\frac{\sum_i \mathrm{jet}_i(p_{\mathrm{T}})+\mathrm{lepton}(p_{\mathrm{T}})}{\sum_i \mathrm{jet}_i(p)+\mathrm{lepton}(p)}$. For SUSY events we expect this variable to be shifted towards higher values, while SM backgrounds are less central. Events are selected that satisfy centrality > 0.6.

After requiring the transverse mass, M_{T}, of the system consisting of the lepton and the missing momentum vector to satisfy $M_{\mathrm{T}} > 260\,\mathrm{GeV}$, the background arises predominantly from two sources: $\mathrm{t}\bar{\mathrm{t}}$ events in which both W bosons decay leptonically but one lepton is lost, and diboson events. In order to suppress the $\mathrm{t}\bar{\mathrm{t}}$ background, we require $M_{\mathrm{T2}}^{\mathrm{W}}$, defined as the minimum "mother" particle mass compatible with all the transverse momenta and mass-shell constraints [58], to be above 260 GeV. By construction, for the dilepton $\mathrm{t}\bar{\mathrm{t}}$ background without mismeasurement effects, $M_{\mathrm{T2}}^{\mathrm{W}}$ has an endpoint at the top quark mass. Figure 9 contains the $\Delta\phi$, centrality, M_{T}, and the $M_{\mathrm{T2}}^{\mathrm{W}}$ distributions after all previously mentioned selection criteria are applied, except on the variables themselves.

Table 6 shows the expected number of SM background and SUSY signal events after each step of the event selection. From left to right STC, STOC, NM1, NM2, and NM3 are shown. We also quote the expected discovery significance assuming either 15% or 25% uncertainty, which is based on the search performed at 8 TeV [35]. Assuming an improved uncertainty of 15% we reach a 5σ discovery level for all models except STOC. Increasing the requirement on $E_{\mathrm{T}}^{\mathrm{miss}}$ to be above 800 GeV improves the sensitivity significantly for the STOC model. In this region of the phase space, we expect to see 11 SM background events and 39 signal events. Larger uncertainties are expected for this selection and a discovery at the 5σ is possible with about $1600\,\mathrm{fb}^{-1}$ assuming 25% systematic uncertainty. Figure 10 shows this significance graphically as a function of integrated luminosity for the different models.

While the search targets direct top squark pair production, the final composition of the selected events depends on the ewkino structure of the model. In the STC model we estimate that about 70% of the expected events contain direct production of top squarks. In this model the main

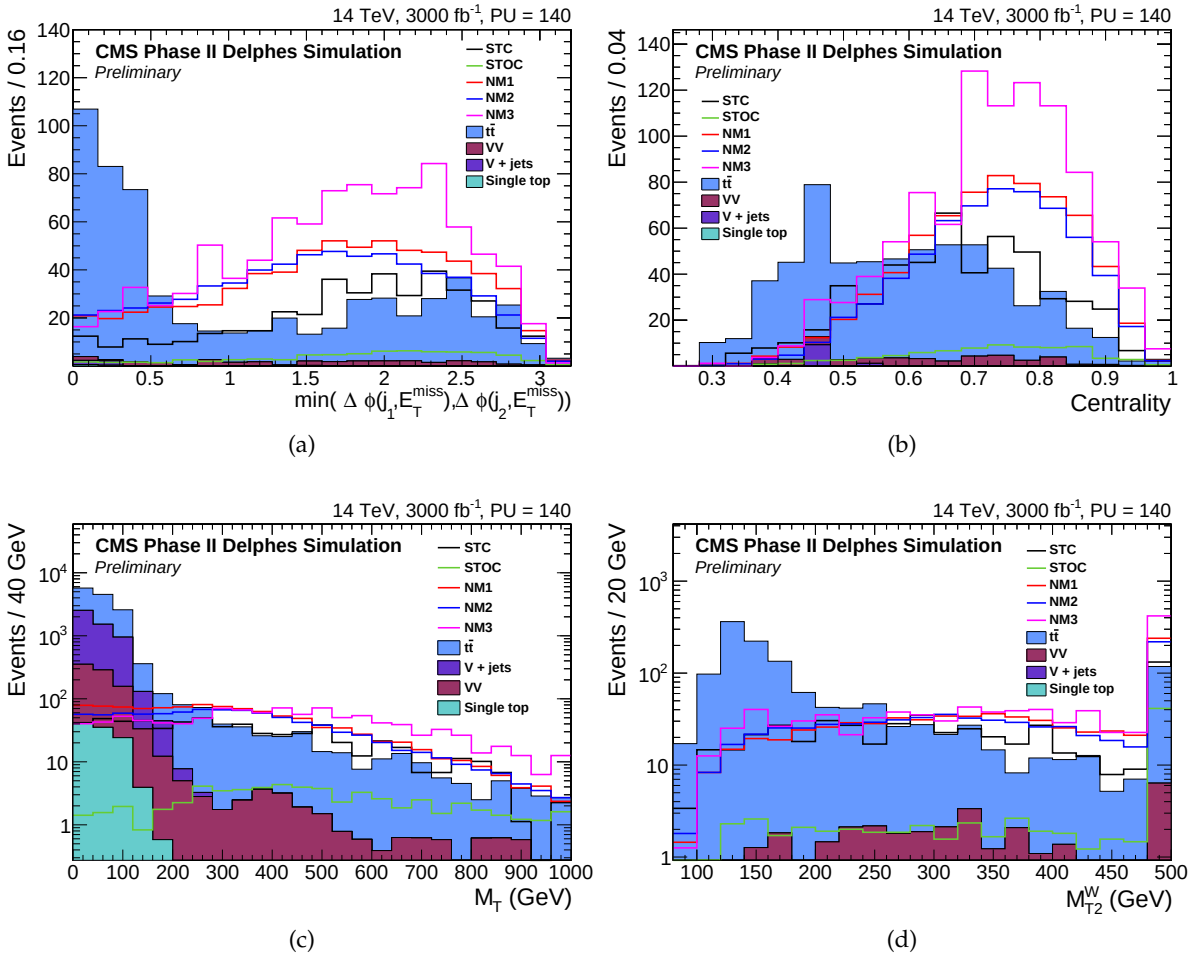

Figure 9: Search for direct stop production in the single-lepton channel: Comparison of (a) $\Delta\phi$, (b) centrality, (c) M_{T}, and (d) $M_{\mathrm{T2}}^{\mathrm{W}}$ for signals and SM backgrounds after all selection requirements are applied except on the variables themselves.

intrinsic background contribution arises from bottom-squark pair production. In the case of the natural models the signal composition is quite diverse and only about 10–25% of the events arise from pair-produced top squarks. Figure 11(a) shows the H_{T} distribution for the expected SM background and overlays the different distributions for the signal models. In Fig. 11(b), the signal composition for the model NM1 is illustrated. The different production modes are separated from each other and added on top of the the SM background. The tail is predominately populated by events arising from $\tilde{\mathrm{q}}\tilde{\mathrm{g}}$ and $\tilde{\mathrm{q}}\tilde{\mathrm{q}}$ production. At $H_{\mathrm{T}} > 2.4\,\mathrm{TeV}$, the fraction of $\tilde{\mathrm{q}}\tilde{\mathrm{g}}$ and $\tilde{\mathrm{q}}\tilde{\mathrm{q}}$ production events is about 80% of the total signal, and the total signal yield is about 50 events which will be clearly observable on top of about 5 expected SM background events, yielding sensitivity to the first- and second-generation squarks with masses about 3 TeV.

The search presented here is sensitive to a variety of different models. However, a definitive statement on whether pair-produced top squarks are the source of the excess of events is very difficult. If the gluino mass is rather low, as in the NM1–NM3 models, processes involving gluinos and first- and second-generation squarks will dominate as an intrinsic SUSY background. Kinematically these events populate the tails of distributions such as H_{T} and $E_{\mathrm{T}}^{\mathrm{miss}}$, and an observed excess should persist when the requirements on these variables are tightened, while a signal caused by direct top squark production might vanish eventually.

Table 6: Search for direct stop production in the single-lepton channel: The event yields for the inclusive signal samples and several SM processes with 3000 fb^{-1} at 14 TeV with 140 pileup interactions. The significances are determined by considering a systematic uncertainty on the background prediction of 15% and 25%. For the high $E_{\mathrm{T}}^{\mathrm{miss}}$ search region, only 25% systematic uncertainty is considered as discussed in the text.

Selection	Total SM	STC	STOC	NM1	NM2	NM3
Exactly 1 e or μ	6160000000	271000	5170	88200	45600	12800
$N_{\mathrm{jets}} \geq 5$	44900000	6550	361	6830	9380	5500
$N_{\text{b-jets}} = 1$ or 2	27700000	4370	259	3980	4830	3210
$E_{\mathrm{T}}^{\mathrm{miss}} > 400\,\mathrm{GeV}$	108000	1610	146	2070	1970	2150
$\Delta\phi > 0.8$	84300	1420	127	1760	1630	1840
Centrality >0.6	48200	1050	99	1460	1350	1510
$M_{\mathrm{T}} > 260\,\mathrm{GeV}$	1320	523	77	733	702	1020
$M_{\mathrm{T2}}^{\mathrm{W}} > 260\,\mathrm{GeV}$	291	349	61	563	518	794
Significance ($\delta B/B = 15\%$)		5.6	1.1	8.2	7.7	10.5
Significance ($\delta B/B = 25\%$)		3.4	0.6	5.0	4.7	6.4
$E_{\mathrm{T}}^{\mathrm{miss}} > 800\,\mathrm{GeV}$	11	–	39	–	–	–
Significance ($\delta B/B = 25\%$)		–	5.7	–	–	–

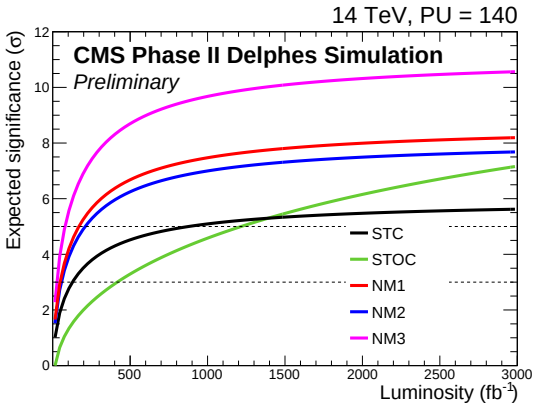

Figure 10: Search for direct stop production in the single-lepton channel: Significance for the different full-spectrum SUSY models. An uncertainty of 15% is used for the curves of NM1, NM2, NM3, and STC, while a higher uncertainty of 25% is chosen for the STOC model due to the increased $E_{\mathrm{T}}^{\mathrm{miss}}$ threshold.

10 Search for compressed supersymmetry spectra in the monojet signature

This section describes a search for compressed supersymmetry spectra in the signature with a high p_{T} jet and large missing transverse momentum. In the stop coannihilation (STOC) model discussed in Section 4, the mass of the top squark is very close to the mass of the $\widetilde{\chi}_1^0$, and normally dominant decays such as $\widetilde{\mathrm{t}}_1 \to \mathrm{t}\widetilde{\chi}_1^0$ and $\widetilde{\mathrm{t}}_1 \to \mathrm{Wb}\widetilde{\chi}_1^0$ are kinematically forbidden. Since the mass of the $\widetilde{\chi}_1^{\pm}$ is above that of $\widetilde{\mathrm{t}}_1$ in the STOC model, the $\widetilde{\mathrm{t}}_1$ cannot decay via an on-shell $\widetilde{\chi}_1^{\pm}$ either, and the loop process $\widetilde{\mathrm{t}}_1 \to \mathrm{c}\widetilde{\chi}_1^0$ becomes the dominant $\widetilde{\mathrm{t}}_1$ decay mode.

The detection of the $\widetilde{\mathrm{t}}_1 \to \mathrm{c} + \widetilde{\chi}_1^0$ decay is challenging experimentally, because the small $\widetilde{\mathrm{t}}_1$-$\widetilde{\chi}_1^0$ mass splitting leads to a very low momentum charm quark, which is essentially undetectable.

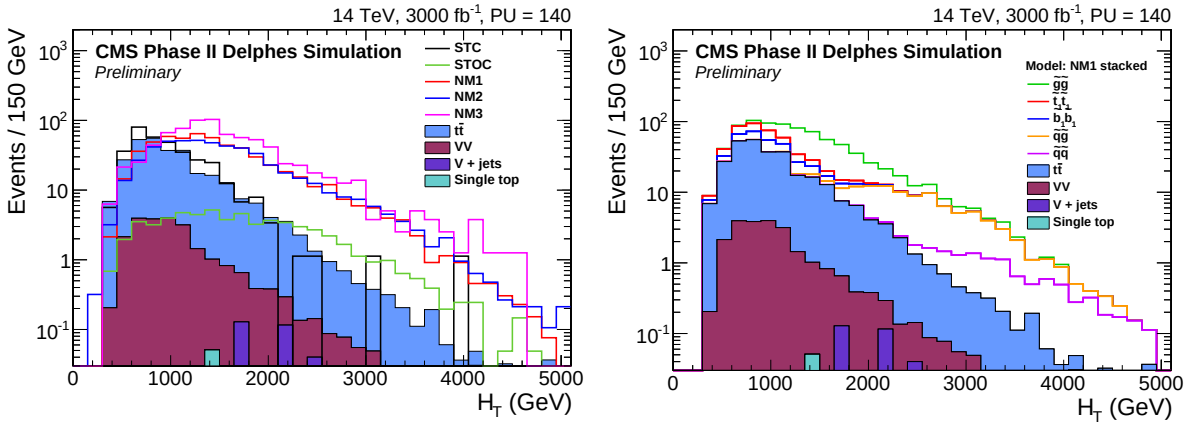

(a) (b)

Figure 11: Search for direct stop production in the single-lepton channel: Comparison of the H_T distribution for signals and SM backgrounds after all selection requirements. In Fig. (a), H_T distributions for the different SUSY scenarios are overlaid, while in Fig. (b) the signal composition is shown for the NM1 model, where the different production modes are separated from each other and stacked on top of the the SM background. At high values of H_T we are sensitive to first two generation squarks with masses above 3 TeV.

The neutralino is completely undetectable. This $\tilde{t}_1$ signature can be still detected if it is accompanied by a high p_T jet arising from initial-state radiation (ISR) together with the missing transverse momentum associated with the two neutralinos. Searches for this monojet-like signature have been performed by CMS and ATLAS using Run 1 data [36, 59].

We investigate the discovery sensitivity of this $\tilde{t}_1$ signature in the STOC model discussed in Section 4 in the LHC Run 2+3 and with the HL-LHC using the search strategy based on the one used in the search performed on the 8 TeV data [36]. We require a leading jet with $p_T > 110\,\text{GeV}$ and $|\eta| < 2.4$ and veto events with a third jet with $p_T > 100\,\text{GeV}$. When there is a second highest p_T jet with $p_T > 60\,\text{GeV}$ and $|\eta| < 4.5$, we require $|\Delta\phi(j1, j2)| < 1.8$ in order to suppress QCD multijet events. As events with a second jet are allowed when they satisfy the above $\Delta\phi(j1, j2)$ requirement, the selected events are not strictly monojet events; however, the term monojet is used as search regions are defined with high p_T thresholds on leading jets, while there is no p_T requirement on second jets. In order to reduce W and top quark backgrounds, events are rejected if there is an identified electron with $p_T > 10\,\text{GeV}$ and $|\eta| < 2.5$ or an identified muon with $p_T > 10\,\text{GeV}$ and $|\eta| < 2.4$ or an identified tau with $p_T > 20\,\text{GeV}$ and $|\eta| < 2.3$ in the event. Events are required to have $E_T^{\text{miss}} > 600\,\text{GeV}$ which helps to reduce QCD multijet background events. Finally we consider multiple search regions with a range of thresholds on the p_T of the leading jet, and the best significance is obtained with the threshold of 900 GeV. The event yields for the SM processes and the STOC $\tilde{t}_1 \to c\tilde{\chi}_1^0$ signal are shown in Table 7.

The leading jet p_T distributions expected with $3000\,\text{fb}^{-1}$ for the signal and background are shown in Fig. 12(a). The signal will appear as broad excess in this distribution, and the accurate determination of the background will be the key for this search. The dominant background arises from Z + jets with $Z \to \nu\bar{\nu}$, which is irreducible. Additional contributions arise from W + jets or $t\bar{t}$ production with $W \to \ell\nu$; such events can have large missing transverse momentum and can satisfy the selection requirements if the lepton is missed.

The projected uncertainty on the background estimation, which is a critical input to the sig-

Table 7: Search in the monojet signature: Background and signal event yields corresponding to 3000 fb^{-1}. The pre-selection refers to events passing all the requirements except the final tight selection on the leading jet p_{T} and $E_{\mathrm{T}}^{\mathrm{miss}}$.

Selection	$\mathrm{Z}(\nu\bar{\nu})$ + jets	$\mathrm{W}(\ell\nu)$ + jets	$\mathrm{t\bar{t}}$	VV	Other	Total SM	STOC
Pre-selection	$7.1 \cdot 10^7$	$5.0 \cdot 10^7$	$6.3 \cdot 10^6$	$2.5 \cdot 10^6$	$1.2 \cdot 10^7$	$14.2 \cdot 10^7$	$8.1 \cdot 10^5$
$E_{\mathrm{T}}^{\mathrm{miss}} > 600\,\mathrm{GeV}$	430000	102000	6440	27600	40700	606000	55700
$p_{\mathrm{T}}(j_1) > 900\,\mathrm{GeV}$	25800	5340	199	1950	1120	34400	6530

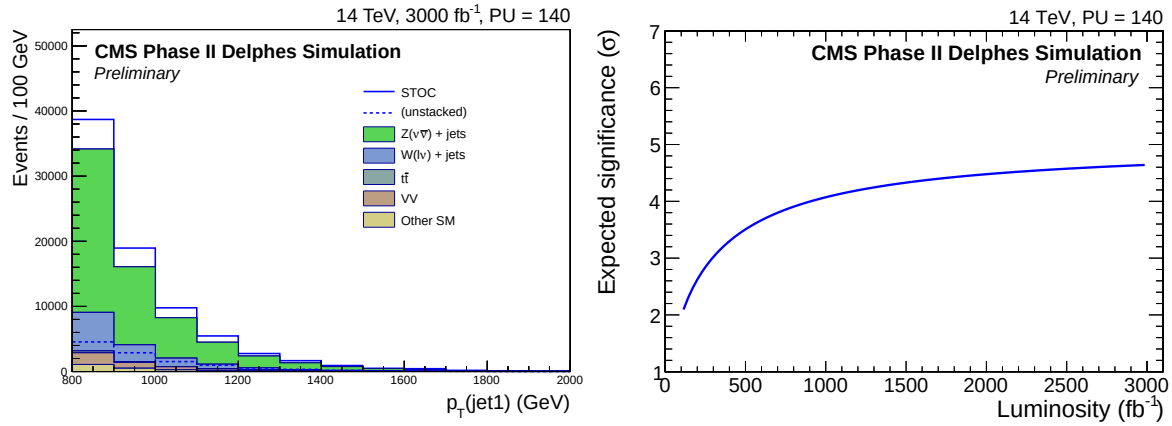

(a) (b)

Figure 12: Search in the monojet signature: (a) Leading jet p_{T} for 3000 fb^{-1} after the selection given in the text except for the requirement on the leading jet p_{T} itself and (b) the discovery significance as a function of the integrated luminosity.

nificance determination, is evaluated as follows. One of the most robust ways to determine the $Z \to \nu\bar{\nu}$ background is to measure the $Z \to \mu^+\mu^-$ event rate and then translate it to the $Z \to \nu\bar{\nu}$ rate based on $N(Z \to \nu\bar{\nu}) = \frac{N^{\mathrm{obs}} - N^{\mathrm{bgd}}}{A \times \epsilon} \cdot R$, where N^{obs} is the number of dimuon events observed, N^{bgd} is the estimated number of background evens contributing to the dimuon sample, A is the acceptance, and ϵ is the selection efficiency for the event. The ratio $R = \mathcal{B}(Z \to \nu\bar{\nu})/\mathcal{B}(Z \to \mu^+\mu^-) = 5.942 \pm 0.019$. The value of $A \times \epsilon$ is typically around 0.68 [36]. The uncertainty in this method arises from the background subtraction, the acceptance determination, R, the lepton efficiency determination, and the statistical uncertainty of N^{obs}. These uncertainty values are estimated based on the 8 TeV analysis [36] and the expected high statistics data in Run 2+3 and HL-LHC. These lead to a total uncertainty on $N(Z \to \nu\bar{\nu})$ of 7% for 300 fb^{-1} and 4% for 3000 fb^{-1}. For the $\mathrm{W}(\ell\nu)$ + jets background, we will use a single lepton control sample to determine this background yield. The uncertainty arises from the acceptance, background subtraction, and the control sample statistics. The total uncertainty is assumed to be about 7% based on the 8 TeV analysis. For the other processes, 25% of the yields are taken as the uncertainty, which is conservative but has a negligible effect on the discovery sensitivity.

The expected significance of this search for $\tilde{\mathrm{t}}_1 \to \mathrm{c} + \tilde{\chi}_1^0$ as a function of the integrated luminosity is shown in Fig. 12(b). The significance is about 3σ with 300 fb^{-1} and it increases to 4.6σ with 3000 fb^{-1}. The clear indication of this direct top squark pair production signal together with the gluino-induced signature in the H_{T}-$H_{\mathrm{T}}^{\mathrm{miss}}$ and single-lepton analyses presented in Sections 6 and 9 would provide a lot of information about the SUSY particle spectrum in this STOC

Table 8: Search for a kinematic edge: Event yields for the SM background processes and the signals expected from the NM1 model for 3000 fb^{-1}. The "Edge" row is for events satisfying $20 < m_{\ell^+\ell^-} < 70$ GeV and the requirement that leptons be same flavor.

Selection	$t\bar{t}$	V + jets	Single top	VV	Other	Total SM	$\widetilde{\chi}_2^0 \to \ell^+\ell^-\widetilde{\chi}_1^0$	$\widetilde{\chi}_4^0 \to \ell^+\ell^-\widetilde{\chi}_1^0$	Other NM1
$N_{\text{jets}} \geq 6$	$1.3 \cdot 10^8$	$1.6 \cdot 10^8$	$4.2 \cdot 10^6$	$1.0 \cdot 10^7$	$1.8 \cdot 10^6$	$3.0 \cdot 10^8$	572	220	20900
$H_{\text{T}} > 1250$ GeV	$4.7 \cdot 10^6$	$9.0 \cdot 10^6$	$3.1 \cdot 10^5$	$3.7 \cdot 10^5$	$1.2 \cdot 10^5$	$1.4 \cdot 10^7$	371	125	13400
$E_{\text{T}}^{\text{miss}} > 450$ GeV	46400	34700	4490	3210	2230	91000	200	64.5	7060
$N_{\text{b-tags}} \geq 1$	37900	7520	1100	2500	1590	50600	185	59.5	6590
Edge	157	1.4	1.5	4.7	5.5	170	176	17.6	142

model, as discussed in Section 14.3.

11 Search using a kinematic edge in the opposite-sign dilepton mass distribution

In this section, we describe an analysis aimed at measurement of the kinematic edge of the opposite-sign dilepton mass distribution in the NM1 scenario, as introduced in Section 4. This study is similar to the CMS analyses of the 7 and 8 TeV data samples [60, 61].

We search for the decay of a neutralino ($\widetilde{\chi}_2^0$) into sleptons, where the $\widetilde{\chi}_2^0$ itself is produced in the decay chain of a gluino. To select these events, we require at least six jets with $p_{\text{T}} > 40$ GeV and $|\eta| < 2.4$, $E_{\text{T}}^{\text{miss}} > 450$ GeV, $H_{\text{T}} > 1250$ GeV, and at least one b-tagged jet with $p_{\text{T}} > 40$ GeV and $|\eta| < 2.4$. Electron and muon candidates must satisfy $p_{\text{T}} > 10$ GeV, $|\eta| < 2.4$ and not be within the range $1.4 < |\eta| < 1.6$. The leptons must be isolated by satisfying $\Sigma E_{\text{T}}/p_{\text{T}}^{\ell} < 0.15$, where the summation is over all particles within a cone of radius $\Delta R = 0.3$ around the lepton momentum direction and p_{T}^{ℓ} is the lepton transverse momentum. The lepton p_{T} requirement is relatively low in order to cover scenarios in which the small mass splitting between the slepton and the neutralino causes the p_{T} spectrum to be quite soft for the subleading lepton, as in the case of natural model NM1.

To calculate the invariant dilepton mass, $m_{\ell^+\ell^-}$, the highest p_{T} electron or muon is paired with the next highest p_{T} electron or muon with opposite charge that also satisfies $\Delta R > 0.3$ for the two leptons. To suppress low mass resonances, we require $m_{\ell^+\ell^-} > 20$ GeV.

The event sample is divided into two subsamples, according to the flavors of the leptons. Signal events appear exclusively in the same flavor (SF) sample, whereas flavor-symmetric (FS) background processes, such as $t\bar{t}$, populate the SF and opposite flavor (OF) samples equally. Therefore, the SF sample is used as the signal region, while the OF sample is used to estimate the background.

Figure 13(a) shows the $m_{\ell^+\ell^-}$ distributions for both signal and background after all selection requirements (including the SF requirement) are applied. Event yields for the SM background processes and SUSY signals are also shown in Table 8. In addition to the $\widetilde{\chi}_2^0 \to \ell\widetilde{\ell} \to \ell^+\ell - \widetilde{\chi}_1^0$ edge signal, there is another edge signal arising from the $\widetilde{\chi}_4^0 \to \ell\widetilde{\ell} \to \ell^+\ell^-\widetilde{\chi}_1^0$ process. Although we cannot identify this second edge signal in the current analysis, this illustrates the potential richness of a SUSY model which we may discover at the LHC. Figures 13(b) and (c) show a fit to SF and OF $m_{\ell^+\ell^-}$ distributions for the case of a single pseudo-dataset. We performed fits on 1000 such pseudo-datasets in order to accurately determine the expected yield.

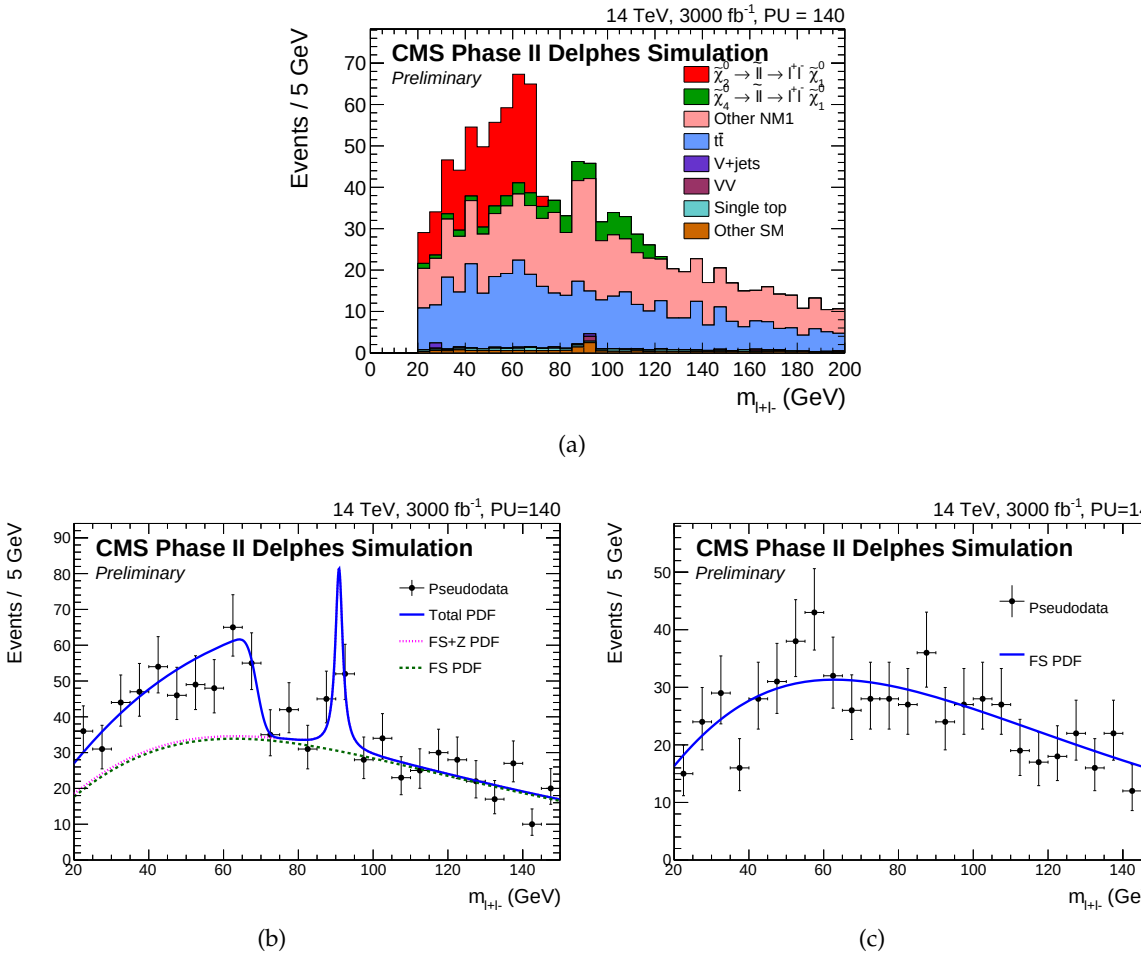

Figure 13: Search for a kinematic edge: Distributions of $m_{\ell^+\ell^-}$ for 3000 fb^{-1} after the selection given in the text. (a) The signal is split between events with a true, properly reconstructed "edge" decay chain and all other signal events. Also shown is an example unbinned fit to the (b) SF and (c) OF dilepton $m_{\ell^+\ell^-}$ distributions. For the SF $m_{\ell^+\ell^-}$ distribution in (b), the solid blue curve is the total PDF, and background components are shown in green and magenta.

Because the $m_{\ell^+\ell^-}$ shape for the edge signal can be derived analytically, the edge signal yield and edge mass can be fitted. An unbinned maximum likelihood fit is performed simultaneously to the SF and OF samples. The SF events are modeled by the sum of probability density functions (PDF) describing the FS background, the Z background, and the edge signal. The OF events are used to constrain the shape of the FS background. The SF FS dilepton background is constrained by the OF dilepton yield by $R(\mathrm{SF/OF}) = 1.00 \pm 0.05$ as done in the 8 TeV analysis [61].

We use the sum of a log-normal distribution and a Gamma distribution to describe the FS events, with the requirements that the two distributions peak in the same place and that the total PDF goes to zero at $m_{\ell^+\ell^-} = 0$. The Z component of the background is fixed except for the overall yield.

Each fit has eight floating parameters: the fraction of the log-normal versus the Gamma distribution, the θ parameter of the Gamma function, the mass of the log-normal + Gamma peak, the FS yield in SF sample, the OF yield, the Z background yield, the mass of the edge and the number of signal events in the $m_{\ell^+\ell^-}$ kinematic edge.

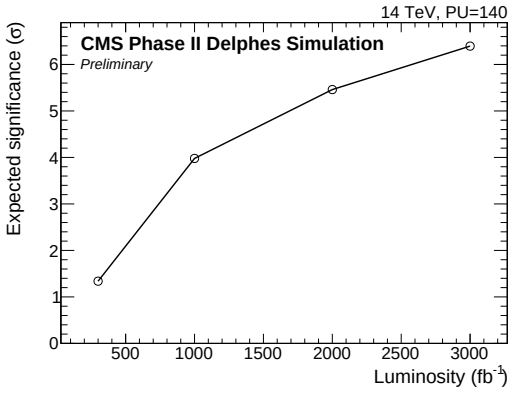

(a)

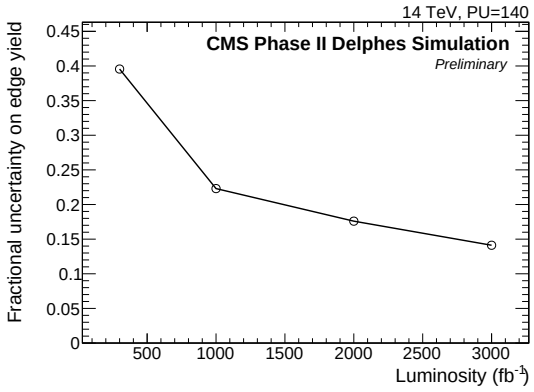

(b)

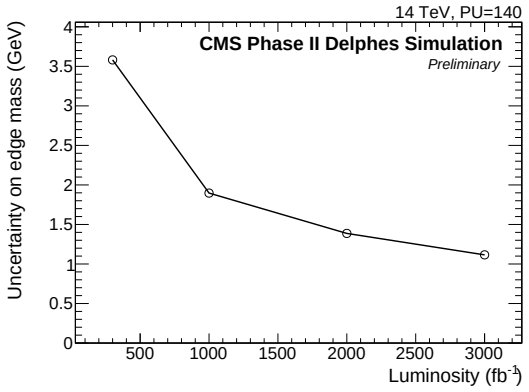

(c)

Figure 14: Search for a kinematic edge: (a) Significance of the $m_{\ell^+\ell^-}$ kinematic edge search from unbinned fits to the SF + OF samples as a function of integrated luminosity, and (b,c) the fractional uncertainty on the $m_{\ell^+\ell^-}$ kinematic edge signal yield and mass as functions of integrated luminosity.

Figure 14 shows the unbinned fit results as a function of luminosity. The significance of the search taking into account the look-elsewhere effect is less than 2σ at $300\,\text{fb}^{-1}$, which grows well in excess of 5σ at $3000\,\text{fb}^{-1}$. The fractional errors on the signal yield and the $m_{\ell^+\ell^-}$ edge mass reduce by a factor of about 3 from $300\,\text{fb}^{-1}$ to $3000\,\text{fb}^{-1}$.

12 Search for supersymmetry in final states with multileptons and b-jets

In this study, we explore a signature with at least three isolated leptons (electrons or muons) and at least two b-jets, targeting the discovery of models with significant b-jet production, including the natural SUSY models (NM1, NM2, and NM3), as well as the stau coannihilation (STC) model. The b-jets can be produced either in the decay chains from direct top squark or bottom squark pair production (yielding two b-jets in the final state) or from gluino pair production, with gluino decay via top or bottom squarks (yielding four b-jets in the final state).

The basic selection requires the presence of three lepton candidates, each with $p_{\text{T}} > 10\,\text{GeV}$ and $|\eta| < 4$. For compatibility with the expected trigger criteria, the leading lepton is required to have $p_{\text{T}} > 25\,\text{GeV}$, while the second leading lepton must have $p_{\text{T}} > 15\,\text{GeV}$. Events are required to have at least two jets satisfying medium b-tagging requirements, as well as

Table 9: Trilepton + b-tag search: Result table for the 3ℓ + b-jets search with $3000\,\text{fb}^{-1}$. This table contains events with at least 3ℓ, $E_{\text{T}}^{\text{miss}} > 500\,\text{GeV}$, and some b-jets.

Selection	Total SM	STC	NM1	NM2	NM3
$N_{\text{b-tags}} = 2$ or 3	27.1 ± 7.3	109	718	204	121
$N_{\text{b-tags}} \geq 4$	0.10 ± 0.04	4.4	134	60	18.3

$p_{\text{T}} > 50\,\text{GeV}$ with $|\eta| < 1.8$. With this selection, the dominant background arises from SM $\text{t}\bar{\text{t}}$ production.

The event sample is then divided into two categories:

- events with either two or three b-tagged jets;
- events with at least four b-tagged jets.

The category with either two or three b-jets is designed for direct top or bottom squark production, whose decays lead to two high-p_{T} b-jets in the final state. In the full-spectrum SUSY models considered here, additional b-jets can arise from Z- or Higgs-boson decays to $\text{b}\bar{\text{b}}$, but these jets are typically softer and are less likely to satisfy the b-tagging requirements. To avoid dependencies on the details of probabilities for lighter-flavored jets to be mistagged as b-jets, events with two or three b-tagged jets are merged into a single category. The category with at least four b-tagged jets is designed for the case of gluino pair production, with each gluino decaying to $\widetilde{\text{t}}_1\text{t}$ or $\widetilde{\text{b}}_1\text{b}$.

Figure 15 shows the $E_{\text{T}}^{\text{miss}}$ distribution for the two b-jet multiplicity categories, 2–3 b-jets and $\geq$4 b-jets, with three identified leptons required in both cases. The requirement $E_{\text{T}}^{\text{miss}} > 500\,\text{GeV}$ suppresses much of the background in the 2–3 b-jet category, and the background is reduced to below the one-event level in the $\geq$4 b-jet category. Table 9 lists the event yields for the background and the four SUSY models considered, assuming an integrated luminosity of $3000\,\text{fb}^{-1}$. The number of signal events varies dramatically across the different signal models. Although the signal typically populates the 2–3 b-jet bin more than the $\geq$4 b-jet bin, the $\geq$4 b-jet requirement gives a large suppression of the background.

The expected signal significance as a function of integrated luminosity is shown in Fig. 16. With a data sample of $3000\,\text{fb}^{-1}$, we expect a significance of at least 5σ for each model. For the NM1 and NM2 models, the sensitivity arises primarily from gluino pair production. Although signal events populate both of the b-jet multiplicity categories, most of the sensitivity for NM1 and NM2 arises from the $\geq$4 b-jet event category. Signals corresponding to these models would be striking and would be discovered within the first $100\,\text{fb}^{-1}$ of data taking. Signal events from the NM3 model are more difficult for this analysis, because the branching fractions of $\widetilde{\text{t}}_1$ and $\widetilde{\text{b}}_1$ to final states including leptons is smaller than for the NM1 and NM2 models. The NM3 model is still discoverable with $200\,\text{fb}^{-1}$ when results from both b-jet categories are combined. The most challenging of these models is STC, where the signal is dominated by top and bottom squark pair production. The 2–3 b-jet category is the key for the discovery of this model, and the signal of this model would be discovered with about $400\,\text{fb}^{-1}$ of integrated luminosity.

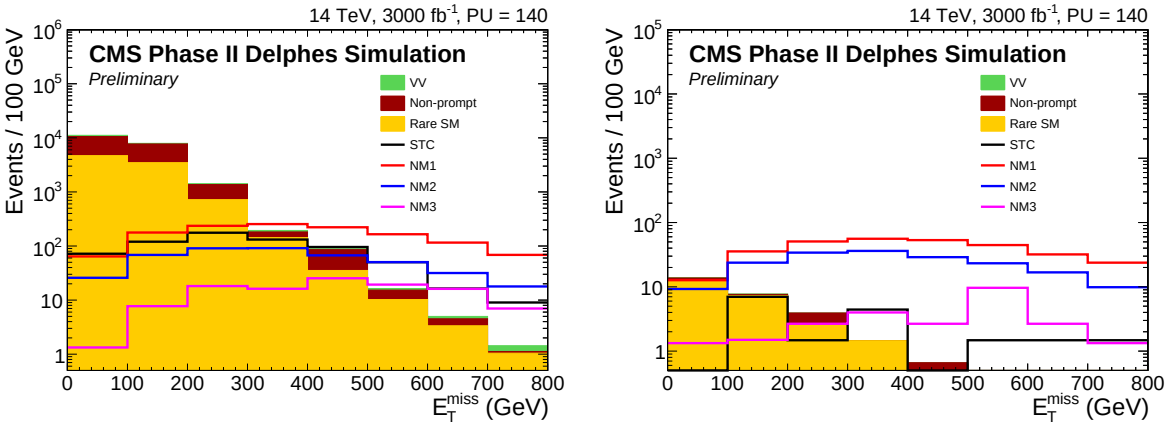

(a) (b)

Figure 15: Trilepton + b-tag search: The $E_{\mathrm{T}}^{\mathrm{miss}}$ distribution for events with (a) 3 ℓ and 2–3 b-tagged jets and (b) 3ℓ and $\geq$4 b-tagged jets. The predictions for the SM background processes and full-spectrum SUSY models are shown.

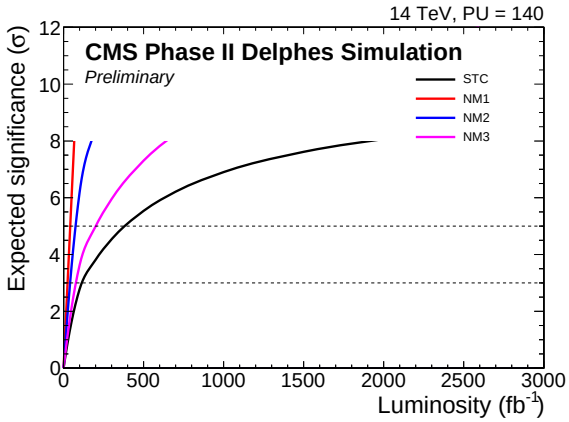

Figure 16: Trilepton + b-tag search: Expected sensitivity versus the integrated luminosity for the models STC, NM1, NM2, and NM3.

13 Search for the electroweak production of charginos and neutralinos

The direct production of neutralinos and charginos takes place through electroweak processes, unlike that for gluinos and squarks. The cross sections for these electroweak processes are typically about two orders of magnitude smaller than the strong production cross sections for particles at the same mass. If the strongly interacting particles are very heavy, however, the searches for neutralinos and charginos can provide the best sensitivity to SUSY particles. Thus, it is important to prepare dedicated searches that target a wide variety of possible signatures associated with these production mechanisms.

We concentrate on the discovery of neutralino-chargino production with the decay modes $\widetilde{\chi}_2^0 \to \mathrm{Z}\widetilde{\chi}_1^0$ or $\widetilde{\chi}_2^0 \to \mathrm{H}\widetilde{\chi}_1^0$, and $\widetilde{\chi}_1^\pm \to \mathrm{W}\widetilde{\chi}_1^0$. We assume that $\widetilde{\chi}_2^0$ and $\widetilde{\chi}_1^\pm$ are mass-degenerate. We determine the discovery sensitivity for two simplified model topologies describing these decays, shown in Fig. 17, and for the full-spectrum SUSY models described in Section 4.

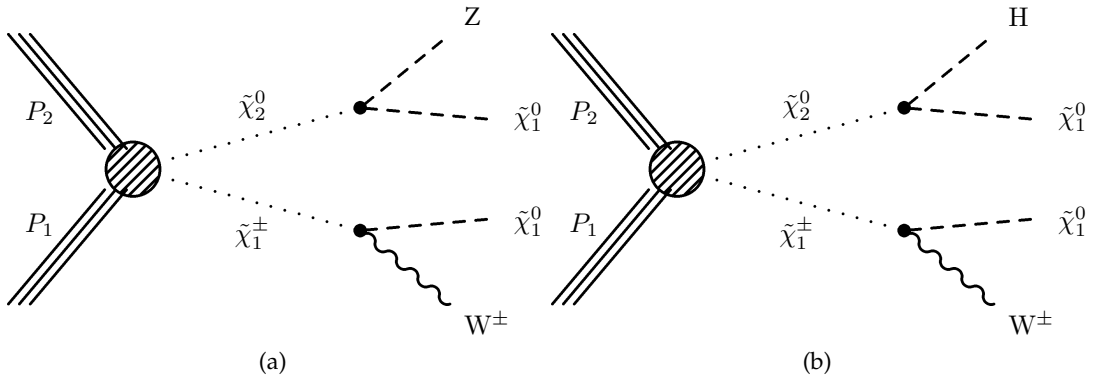

Figure 17: Simplified models for chargino-neutralino production leading to (a) WZ + $E_{\mathrm{T}}^{\mathrm{miss}}$ and (b) WH + $E_{\mathrm{T}}^{\mathrm{miss}}$ final states.

13.1 Search for $\widetilde{\chi}_1^{\pm}\widetilde{\chi}_2^0$ production with $\widetilde{\chi}_1^{\pm} \to W^{\pm}\widetilde{\chi}_1^0$ and $\widetilde{\chi}_2^0 \to Z\widetilde{\chi}_1^0$ in the multilepton channel

The WZ search is performed in the channels where both the Z and the W boson decay to electrons and muons. The analysis method is based on the CMS 8 TeV analysis [19]. Lepton candidates must satisfy $p_{\mathrm{T}} > 10\,\mathrm{GeV}$ and $|\eta| < 4$. For compatibility with the expected trigger requirements, we require the leading lepton and the second leading lepton to satisfy $p_{\mathrm{T}} > 25\,\mathrm{GeV}$ and $p_{\mathrm{T}} > 15\,\mathrm{GeV}$, respectively. We also require one opposite-sign same-flavor (OSSF) lepton pair (e^+e^- or $\mu^+\mu^-$). Events with a fourth lepton or with a b-tagged jet are rejected. The b-jet veto reduces the $\mathrm{t\bar{t}}$ background. In order to improve the sensitivity to models with heavy $\widetilde{\chi}_1^{\pm}$ and $\widetilde{\chi}_2^0$, we add a signal region with a much more stringent object selection, requiring the three leading leptons to satisfy $p_{\mathrm{T}} > 120$, 90, and 40 GeV, respectively. For this signal region, we veto events containing a jet with $p_{\mathrm{T}} > 100\,\mathrm{GeV}$, reducing mostly the non-prompt backgrounds and the WZ background.

The dominant background, accounting for 70% to 95% of SM events in the different signal regions, arises from WZ production. The second most important SM contribution is the so-called non-prompt background, which arises from $\mathrm{t\bar{t}}$ and Drell-Yan + jets events. Backgrounds in this category can only produce two prompt leptons. The third lepton is typically produced in the decay of a heavy quark in a jet, which in rare cases can satisfy the lepton isolation requirements, or it is a fake lepton. The last category of background is associated with rare SM processes that have small cross sections, such as triple boson production.

When calculating the invariant mass of the OSSF pair and more than one possible OSSF pair is possible, we choose the pair with the invariant mass closest to the Z boson mass. The remaining lepton and the missing transverse energy are used to calculate the transverse mass M_{T}. In the signal regions with $M_{\mathrm{T}} > m_{\mathrm{W}}$, the WZ background is efficiently reduced, as for this background the dilepton invariant mass should be near to the Z boson mass, while the transverse mass reaches an endpoint at the mass of the W boson. In SUSY events the additional $E_{\mathrm{T}}^{\mathrm{miss}}$ due to the LSPs can cause the transverse mass to be larger than the W boson mass.

Since some SUSY scenarios produce Z bosons, while others might produce higher invariant dilepton masses, e.g., in slepton decays, it is natural to distinguish between "on-Z" events and "high-Z" events. In on-Z events, the invariant mass of the OSSF pair has to be $75 < m_{\ell^+\ell^-} < 105\,\mathrm{GeV}$, while for high-Z events $m_{\ell^+\ell^-} > 105\,\mathrm{GeV}$ is required. In order to optimize the sensitivity for different SUSY scenarios, we use search regions (SRs) defined by $E_{\mathrm{T}}^{\mathrm{miss}}$ and

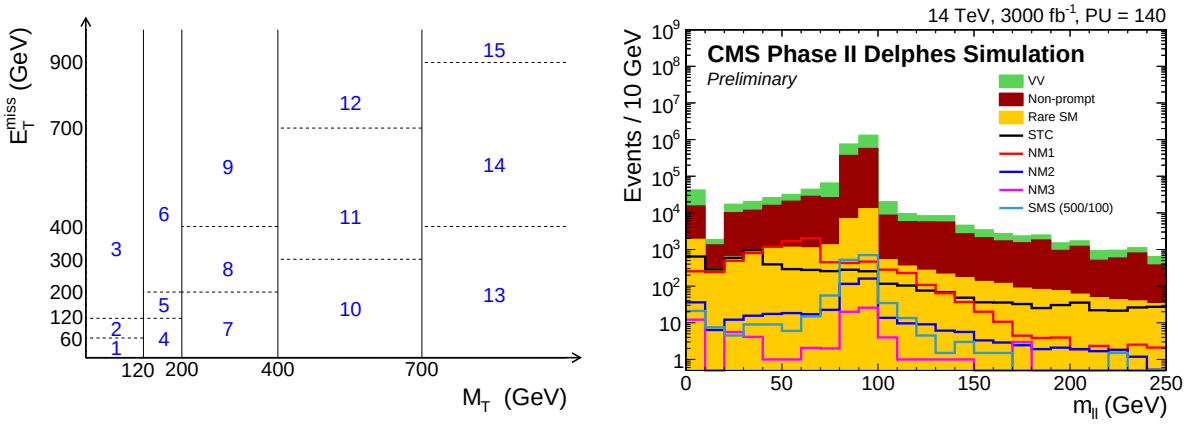

(a) (b)

Figure 18: Multilepton search: (a) Definition of search regions (SRs) and (b) the $m_{\ell^+\ell^-}$ distribution for the different full-spectrum SUSY models compared to the SM background. The SMS signal distribution corresponds to the topology shown in Fig. 17(a) with $m_{\tilde{\chi}_1^\pm} = m_{\tilde{\chi}_2^0} = 500\,\text{GeV}$ and $m_{\tilde{\chi}_1^0} = 100\,\text{GeV}$.

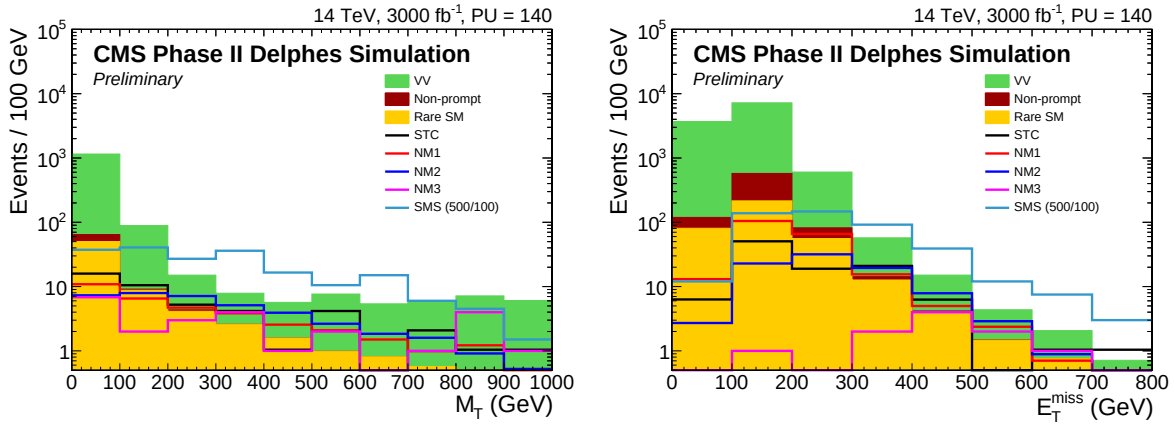

(a) (b)

Figure 19: Multilepton search: Distributions for the on-Z search region SR 9: (a) the M_T distribution for events with $E_\text{T}^\text{miss} > 400\,\text{GeV}$ and (b) the E_T^miss distribution for events with $200 < M_\text{T} < 400\,\text{GeV}$. The SMS signal distributions correspond to the topology shown in Fig. 17(a) with $m_{\tilde{\chi}_1^\pm} = m_{\tilde{\chi}_2^0} = 500\,\text{GeV}$ and $m_{\tilde{\chi}_1^0} = 100\,\text{GeV}$.

M_T, as shown in Fig. 18(a). The invariant mass distribution of the OSSF pair for the different full-spectrum SUSY models compared to the background is given in Fig. 18(b). Figure 19 show E_T^miss and M_T distributions for the on-Z signal region SR 9.

We assume 3% uncertainty for the efficiency to reconstruct each lepton in the event and 1% as trigger uncertainty. The largest uncertainty is caused by E_T^miss, which is scaled by $\pm$ 5%. The resulting differences lead to an uncertainty of about 10% in the low E_T^miss SRs, rising up to 25% in the high E_T^miss SRs. The uncertainty due to the Monte Carlo statistics is in most cases below 5%, but for a very few bins they can have an influence.

Table 10 contains the results for the different search regions, comparing the estimated total SM

background to the different SUSY models, including the simplified model with $m_{\tilde{\chi}_1^{\pm}} = m_{\tilde{\chi}_2^0} = 500\,\text{GeV}$ and $m_{\tilde{\chi}_1^0} = 100\,\text{GeV}$.

The results are interpreted in different SUSY scenarios using the asymptotic option of the Higgs combination tool [48]. For the SMS we test a matrix of mass points in steps of 100 GeV, ranging from 100 to 1000 GeV for $m_{\tilde{\chi}_1^{\pm}} = m_{\tilde{\chi}_2^0}$, and from 0 to 900 GeV for $m_{\tilde{\chi}_1^0}$ (with the requirement $m_{\tilde{\chi}_1^{\pm}} = m_{\tilde{\chi}_2^0} > m_{\tilde{\chi}_1^0}$). The corresponding 5σ discovery lines for $300\,\text{fb}^{-1}$ with the Phase I detector and 50 pileup events, and $3000\,\text{fb}^{-1}$ with the Phase II detector and 140 pileup events, are shown in Fig. 20(a) for branching fractions of $\mathcal{B}(\tilde{\chi}_2^0 \to Z\tilde{\chi}_1^0) = 50\%$ and 100%. For high $\tilde{\chi}_1^{\pm}$ and $\tilde{\chi}_2^0$ masses, the sensitivity is strongest in the signal region with tight lepton p_T requirements. Figure 20(b) contains the discovery sensitivity as function of the luminosity for the investigated full-spectrum SUSY models. We reach about 3–4σ for the STC, NM1, and NM2 models, and about 2σ for the NM3 model.

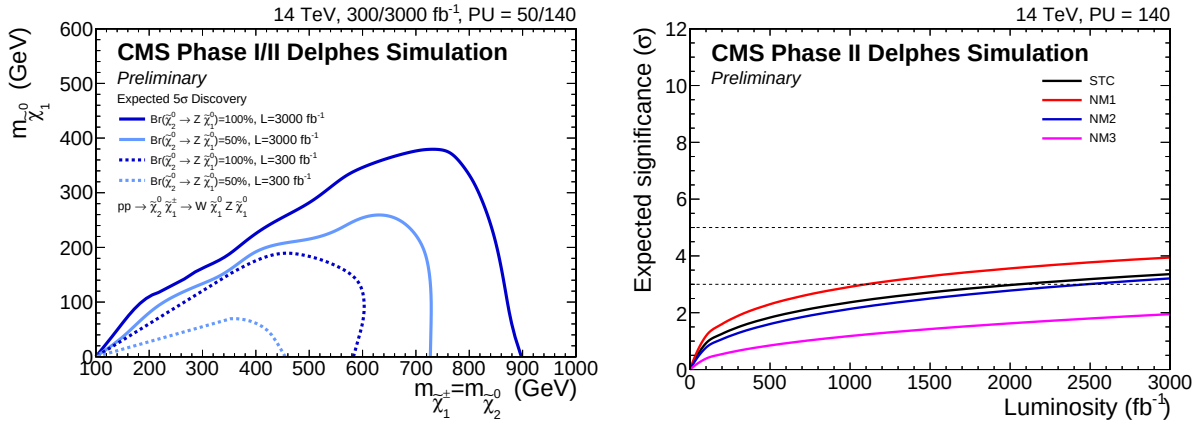

(a) (b)

Figure 20: Multilepton search: (a) Contours for 5σ discovery in the SMS model with $m_{\tilde{\chi}_1^{\pm}} = m_{\tilde{\chi}_2^0}$ versus $m_{\tilde{\chi}_1^0}$ plane. (b) Discovery significance as a function of the integrated luminosity.

13.2 Search for $\tilde{\chi}_1^{\pm}\tilde{\chi}_2^0$ production in the WH + E_T^{miss} final state

This search targets chargino-neutralino production leading to WH + E_T^{miss} final states, as shown in Fig. 17(b). We search for this topology using $W \to \ell\nu$ and $H \to b\bar{b}$, which has the largest branching fraction of any Higgs decay. This single lepton channel was found to be the most sensitive in the 8 TeV run [19].

Events are required to contain a single isolated high p_T lepton (e or μ), as well as two high p_T b jets that reconstruct to the mass of a Higgs boson. The lepton candidate is required to satisfy $p_T > 40\,\text{GeV}$ and $|\eta| < 2.4$. Events are vetoed if additional leptons with $p_T > 10\,\text{GeV}$ are present. This veto suppresses $t\bar{t}$ events with two leptons from the decay of the two W bosons. To suppress $t\bar{t}$ events with a single leptonic W decay, events are also vetoed if there are additional jets satisfying $p_T > 30\,\text{GeV}$ and $|\eta| < 2.4$. We require the invariant mass of the two b-tagged jets, $m_{b\bar{b}}$ to lie between 90 and 150 GeV to be consistent with the Higgs boson mass.

The transverse mass, M_T, computed from the lepton momentum and E_T^{miss}, is required to satisfy $M_T > 100\,\text{GeV}$. This cut strongly suppresses backgrounds with exactly one leptonic W boson decay. The contransverse mass, M_{CT}, as defined in Section 8, is used to suppress the remaining $t\bar{t}$ background, which has an endpoint at $M_{CT} = (m_t^2 - m_W^2)/m_t \approx 135\,\text{GeV}$. We require $M_{CT} >$

Table 10: Multilepton search: Event yields for the SM background, the SMS signal with $m_{\widetilde{\chi}_1^\pm} = m_{\widetilde{\chi}_2^0} = 500\,\text{GeV}$ and $m_{\widetilde{\chi}_1^0} = 100\,\text{GeV}$, and the investigated full-spectrum SUSY model signals. The results are split into the on-Z and high-Z signal regions.

SR		Total SM	SMS	STC	NM1	NM2	NM3
on-Z	1	1010000 ± 190000	21	97	150	11	0
	2	810000 ± 150000	73	140	250	20	2.0
	3	167000 ± 26000	300	190	310	72	17
	4	99400 ± 8900	41	55	96	12	1.0
	5	41300 ± 9100	66	51	96	18	0
	6	2700 ± 1300	140	53	57	35	3.0
	7	10900 ± 1600	150	57	120	26	1.0
	8	660 ± 230	240	40	81	51	2.0
	9	22.9 ± 6.3	63	9.4	8.5	12	7.0
	10	282 ± 82	50	11	28	12	1.0
	11	72 ± 16	120	7.3	21	22	6.0
	12	0.8 ± 0.3	0	2.1	0.6	0.4	0
	13	21.3 ± 2.0	6.0	2.1	1.6	1.5	1.0
	14	32.9 ± 4.9	21	5.2	3.4	3.8	8.0
	15	1.5 ± 0.4	0	0	0.1	0.1	0
high-Z	1	19200 ± 2300	0	120	72	3.6	0
	2	25900 ± 2700	3.0	230	140	7.2	1.0
	3	11800 ± 2300	15	270	200	18	5.0
	4	3090 ± 410	1.5	30	37	3.4	0
	5	1660 ± 350	1.5	51	41	5.6	0
	6	190 ± 49	4.5	34	39	6.5	1.0
	7	1260 ± 230	4.5	41	51	5.3	0
	8	109 ± 34	7.5	31	35	9.7	1.0
	9	8.0 ± 2.1	4.5	3.1	4.6	1.8	1.0
	10	126 ± 12	4.5	7.4	12	2.0	1.0
	11	14.7 ± 4.5	0	5.3	9.2	2.9	1.0
	12	0.3 ± 0.1	0	0	0.3	0.1	0
	13	14 ± 1.5	0	1.0	1.2	0.2	0
	14	6.8 ± 1.2	0	0	1.2	0.7	0
	15	0.2 ± 0.1	0	0	0.1	0.1	0

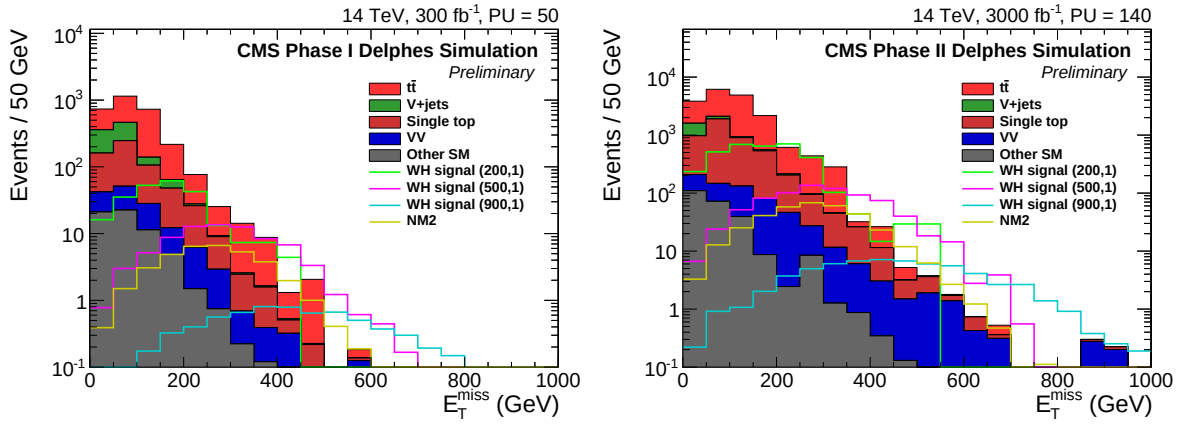

(a) (b)

Figure 21: Ewkino WH search: Distributions of $E_{\mathrm{T}}^{\mathrm{miss}}$ for (a) the Phase I 50 pileup scenario and (b) the Phase II 140 pileup scenario, after all other selections are applied. The WH signal distributions correspond to the SMS topology shown in Fig. 17(b), and the first and second numbers in parentheses indicate the values of $m_{\widetilde{\chi}_1^{\pm}} = m_{\widetilde{\chi}_2^0}$ and $m_{\widetilde{\chi}_1^0}$, respectively.

160 GeV. Finally, signal regions in $E_{\mathrm{T}}^{\mathrm{miss}}$ are defined by the series of thresholds $E_{\mathrm{T}}^{\mathrm{miss}} > 200$, 300, 400, and 500 GeV.

Figure 21 shows the distribution of $E_{\mathrm{T}}^{\mathrm{miss}}$ for the SM backgrounds, compared with those for several simulated signal models. Figure 21(a) shows the Phase I, 50 pileup scenario with 300 fb^{-1}, while the Figure 21(b) shows the Phase II, 140 pileup scenario with 3000 fb^{-1}. Clear separation between signal and background is observed in the $E_{\mathrm{T}}^{\mathrm{miss}}$ distribution for the SMS signals with higher $\widetilde{\chi}_1^{\pm}$ and $\widetilde{\chi}_2^0$ masses for both scenarios.

Table 11 shows the yields for both signal and background in the signal regions for the Phase I scenario with an integrated luminosity of 300 fb^{-1} and 50 pileup events. The signal yields correspond to three simplified model mass points and also to the natural model NM2. Table 12 lists the signal significance for each of these signal models. Two values of the systematic uncertainty for the total background are considered: 25%, corresponding to the total uncertainty in the 8 TeV result, and 12.5%, assuming an improvement on the 8 TeV result. Given that many of the systematic uncertainties in the 8 TeV result were dominated by data control region statistics, it is reasonable to believe these can be reduced with more data. At an integrated luminosity of 300 fb^{-1}, the expected significance values fall below 5σ for all the models shown in Table 12. However, for $\widetilde{\chi}_1^{\pm}$ and $\widetilde{\chi}_2^0$ masses near 400 GeV, the signal exceeds 5σ in significance as shown in Fig. 22(a).

Table 13 shows the yields in the Phase II 140 pileup scenario. Table 14 contains the resulting significance for a few signal points assuming the two values of background systematic uncertainty. Sensitivity to the lower mass points at 5σ is achieved even with the larger systematic uncertainty. The 900 GeV mass point is on the edge of the discovery sensitivity with 25% systematic uncertainty and appears discoverable with lower uncertainty. For NM2 with the $\widetilde{\chi}_1^{\pm}/\widetilde{\chi}_2^0$ mass of about 535 GeV, the maximal significance obtained is 4.7σ with the lower systematic uncertainty, if only the WH decay is investigated. In this model, the branching fractions of $\widetilde{\chi}_1^{\pm}\widetilde{\chi}_2^0 \to (\mathrm{W}\widetilde{\chi}_1^0)(\mathrm{H}\widetilde{\chi}_1^0)$ and $\widetilde{\chi}_1^{\pm}\widetilde{\chi}_2^0 \to (\mathrm{W}\widetilde{\chi}_1^0)(\mathrm{Z}\widetilde{\chi}_1^0)$ are 88% and 12%, respectively. If results of the WZ analysis are added, this scenario will be discoverable with $> 5\sigma$ significance as shown in Fig. 24(b).

Table 11: Ewkino WH search: Yields for the Phase I scenario with 50 pileup events and 300 fb^{-1}, after all signal selections except for the E_T^{miss} requirement listed.

Sample	$E_T^{miss} > 200$ GeV	$E_T^{miss} > 300$ GeV	$E_T^{miss} > 400$ GeV
$t\bar{t}$	87 ± 23	22 ± 10	2.7 ± 1.9
V + jets	2.1 ± 0.4	0.2 ± 0.0	0.0 ± 0.0
single top	29 ± 5	3.3 ± 0.8	0.4 ± 0.1
diboson	8.0 ± 1.8	1.2 ± 0.3	0.4 ± 0.1
Other SM	2.7 ± 0.6	0.5 ± 0.1	0.1 ± 0.0
Total SM	129 ± 24	27 ± 10	3.7 ± 1.9
WH signal (200,1)	75 ± 10	19 ± 5	4.4 ± 2.5
WH signal (500,1)	60 ± 2	34 ± 1	13 ± 1
WH signal (900,1)	6.2 ± 0.1	5.2 ± 0.1	3.8 ± 0.1
Natural Model 2	26 ± 0	13 ± 0	3.7 ± 0.1

Table 12: Ewkino WH search: Estimated significance in σ for a few signal points in the Phase I, 50 pileup scenario with 300 fb^{-1}. The yields from Table 11 are used, and two different choices of background systematic uncertainty are presented.

Sample	$E_T^{miss} > 200$ GeV	$E_T^{miss} > 300$ GeV	$E_T^{miss} > 400$ GeV
	25% Background Uncertainty		
WH signal (200,1)	1.7	1.8	1.5
WH signal (500,1)	1.4	2.9	3.9
WH signal (900,1)	-	0.4	1.3
Natural Model 2	0.6	1.2	1.3
	12.5% Background Uncertainty		
WH signal (200,1)	3.2	2.6	1.8
WH signal (500,1)	2.6	4.4	4.5
WH signal (900,1)	0.2	0.7	1.5
Natural Model 2	1.2	1.8	1.5

Table 13: Ewkino WH search: Yields for the Phase II scenario with 140 pileup events and 3000 fb^{-1}, after all signal cuts except for the E_T^{miss} requirement listed.

Sample	$E_T^{miss} > 200$ GeV	$E_T^{miss} > 300$ GeV	$E_T^{miss} > 400$ GeV	$E_T^{miss} > 500$ GeV
$t\bar{t}$	1000 ± 260	261 ± 130	17 ± 13	0.5 ± 0.2
V + jets	14 ± 4	1.2 ± 0.3	0.1 ± 0.1	0.0 ± 0.0
single top	291 ± 38	66 ± 11	13 ± 4	2.5 ± 0.8
diboson	87 ± 16	24 ± 5	8.4 ± 2.0	4.4 ± 1.4
Other SM	14 ± 5	2.7 ± 0.6	0.6 ± 0.1	0.1 ± 0.0
Total SM	1410 ± 260	354 ± 130	39 ± 14	7.5 ± 1.6
WH signal (200,1)	1340 ± 140	220 ± 57	73 ± 33	29 ± 21
WH signal (500,1)	605 ± 18	367 ± 14	154 ± 9	40 ± 5
WH signal (900,1)	60 ± 1	51 ± 1	38 ± 1	24 ± 1
Natural Model 2	276 ± 4	150 ± 3	46 ± 2	11 ± 1

Figure 22(a) shows the 5σ discovery reach and 95% confidence level (CL) exclusion for each scenario assuming the smaller systematic uncertainty of 12.5%. In the Phase I and 300 fb^{-1} scenario, the 5σ discovery reach includes only a small region around $m_{\tilde{\chi}_2^0} \approx 400$ GeV for LSP masses less than 50 GeV, while the 3000 fb^{-1} Phase II program increases this discovery region

Table 14: Ewkino WH search: Estimated significance in σ for a few signal points in the Phase II, 140 pileup scenario with 3000 fb^{-1}. The yields from Table 13 are used, and two different choices of background systematic uncertainty are presented.

Sample	$E_{\mathrm{T}}^{\mathrm{miss}} > 200$ GeV	$E_{\mathrm{T}}^{\mathrm{miss}} > 300$ GeV	$E_{\mathrm{T}}^{\mathrm{miss}} > 400$ GeV	$E_{\mathrm{T}}^{\mathrm{miss}} > 500$ GeV
	25% Background Uncertainty			
WH signal (200,1)	2.8	1.9	4.3	5.5
WH signal (500,1)	1.4	3.0	7.6	6.9
WH signal (900,1)	-	0.4	2.5	4.7
Natural Model 2	0.6	1.3	2.9	2.4
	12.5% Background Uncertainty			
WH signal (200,1)	5.8	3.8	6.7	6.8
WH signal (500,1)	2.9	5.9	12	8.6
WH signal (900,1)	-	0.9	3.9	5.8
Natural Model 2	1.4	2.7	4.7	3.0

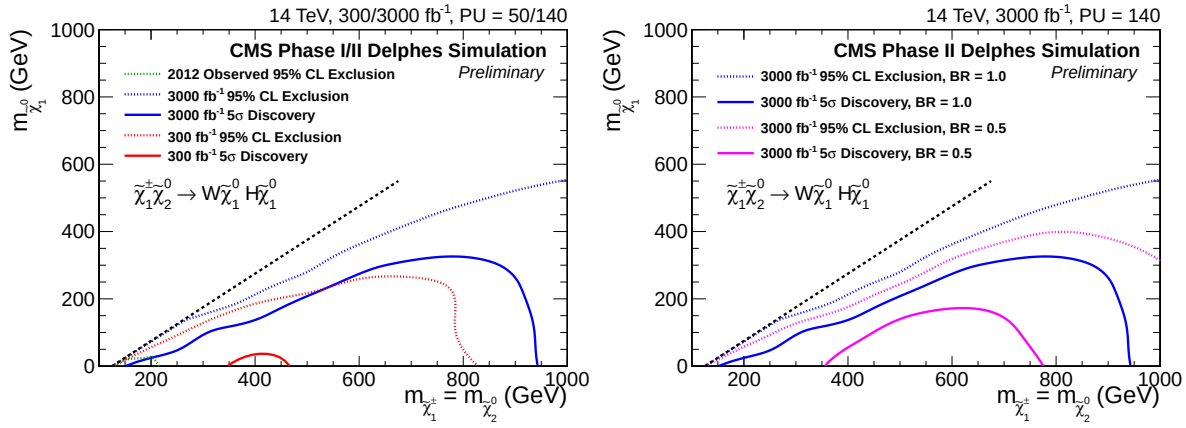

(a) (b)

Figure 22: Ewkino WH search: (a) Contours for 5σ discovery and 95% CL exclusion in the SMS plane of $m_{\widetilde{\chi}_1^{\pm}} = m_{\widetilde{\chi}_2^0}$ versus $m_{\widetilde{\chi}_1^0}$ for the Phase I 50 pileup and Phase II 140 pileup scenarios, assuming a background systematic uncertainty of 12.5%. The observed exclusion contour based on the 2012 data is also overlaid. (b) The same contours in the Phase II 140 pileup scenario, showing the impact of different branching fractions for $\widetilde{\chi}_1^{\pm}\widetilde{\chi}_2^0 \to (\mathrm{W}\widetilde{\chi}_1^0)(\mathrm{H}\widetilde{\chi}_1^0)$.

dramatically up to 950 GeV for LSP masses up to 300 GeV. The exclusion region covers $\widetilde{\chi}_1^{\pm}$ and $\widetilde{\chi}_2^0$ masses up to about 800 GeV for LSP masses of up to about 250 GeV in the Phase I and 300 fb^{-1} scenario. If no signal is observed with the HL-LHC data, the limits will extend beyond 1 TeV for $\widetilde{\chi}_1^{\pm}$ and $\widetilde{\chi}_2^0$ masses with LSP masses up to about 550 GeV. Figure 22(b) shows the impact of a 50% branching fraction for $\widetilde{\chi}_1^{\pm}\widetilde{\chi}_2^0 \to (\mathrm{W}\widetilde{\chi}_1^0)(\mathrm{H}\widetilde{\chi}_1^0)$. The discovery sensitivity is reduced to the range of $\widetilde{\chi}_1^{\pm}$ between 400 and 750 GeV and extends up to an LSP mass of about 150 GeV.

As this analysis is highly dependent on high luminosity, we investigate here the effect of a possible continuation of running without an extensive upgrade of the detector, which would lead to a serious aging effect even if the pixel detector is replaced after 300–500 fb^{-1}. A maximum luminosity of 1000 fb^{-1} is expected to be taken until crucial detector parts, especially the tracker and the endcaps, suffer from significant radiation damage. The effect of the degradation in the lepton identification, b-tagging efficiency, and $E_{\mathrm{T}}^{\mathrm{miss}}$ resolution have been estimated,

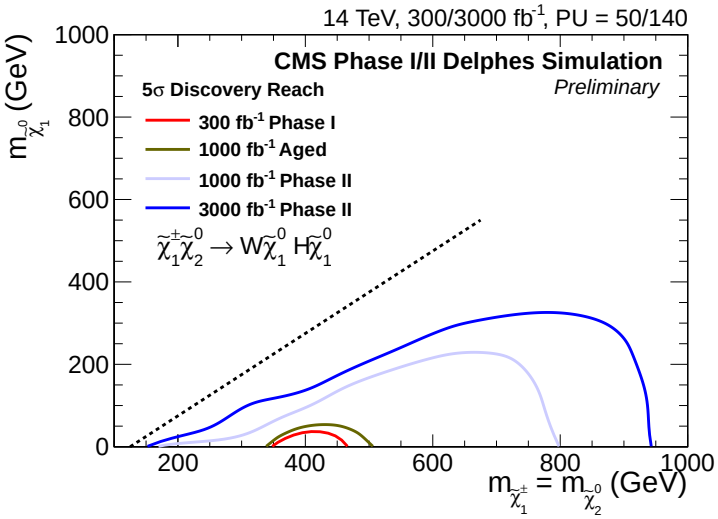

Figure 23: Ewkino WH search: Contours for 5σ discovery in the SMS plane of $m_{\widetilde{\chi}_1^\pm} = m_{\widetilde{\chi}_2^0}$ versus $m_{\widetilde{\chi}_1^0}$ for scenarios of $300\,\text{fb}^{-1}$ with the Phase I detector and 50 pileup interactions, $1000\,\text{fb}^{-1}$ with the aged detector and 140 pileup interactions, and both $1000\,\text{fb}^{-1}$ and $3000\,\text{fb}^{-1}$ with the Phase II detector and 140 pileup interactions.

and the lepton (e and μ) efficiency and b-tagging efficiency are reduced by 0.84 and 0.67, respectively, and the missing E_T resolution is degraded by 40 GeV in the DELPHES simulation for the Phase II 140 pileup scenario. In addition, the difference with and without the track trigger at level-1 is investigated by raising the electron p_T threshold from 40 to 50 GeV and restricting muons to $|\eta| < 1.1$, as the trigger rate would be too high without these tighter requirements without using tracks at the level-1 trigger level.

The results are summarized in Fig. 23. Continued operation to accumulate $1000\,\text{fb}^{-1}$ with a degraded detector extends the discovery reach only marginally beyond the sensitivity with $300\,\text{fb}^{-1}$ of data, while at $1000\,\text{fb}^{-1}$ with the Phase II detector, the discovery reach is extended substantially. This provides a clear demonstration of how important the detector upgrade can be.

For models where $\widetilde{\chi}_2^0$ decays to either $\text{Z}\widetilde{\chi}_1^0$ or $\text{H}\widetilde{\chi}_1^0$, it is possible to enhance the discovery sensitivity by combining the WZ + E_T^miss and WH + E_T^miss searches. The results of this combination are shown in Fig. 24(a) for the branching fraction of $\mathcal{B}(\widetilde{\chi}_2^0 \to \text{Z}\widetilde{\chi}_1^0) = \mathcal{B}(\widetilde{\chi}_2^0 \to \text{H}\widetilde{\chi}_1^0) = 50\%$, as well as for $\mathcal{B}(\widetilde{\chi}_2^0 \to \text{Z}\widetilde{\chi}_1^0) = 100\%$ and $\mathcal{B}(\widetilde{\chi}_2^0 \to \text{H}\widetilde{\chi}_1^0) = 100\%$. As shown in Figs. 20(a) and 22(b), the sensitivities from the individual WZ + E_T^miss and WH + E_T^miss searches are reduced significantly when the branching fraction of the targeted decay channel is 50% instead of 100%. However, by combing the searches in the two channels, we can extend the discovery sensitivity up to $m_{\widetilde{\chi}_1^\pm} = m_{\widetilde{\chi}_2^0} = 500\,\text{GeV}$ for $\widetilde{\chi}_1^0$ masses up to 100 GeV with a luminosity of $300\,\text{fb}^{-1}$. With $3000\,\text{fb}^{-1}$, this can be significantly extended up to $m_{\widetilde{\chi}_2^0} = m_{\widetilde{\chi}_1^\pm} = 850\,\text{GeV}$ for $\widetilde{\chi}_1^0$ masses up to 300 GeV, almost reaching the sensitivity that could be achieved if one channel would be favored with a branching fraction of 100%. The discovery sensitivity for the natural model NM2 is below 5σ if both channels are investigated separately, but a combined analysis will be able to discover the $\widetilde{\chi}_1^\pm \widetilde{\chi}_2^0$ production in this model, as shown in Fig. 24(b).

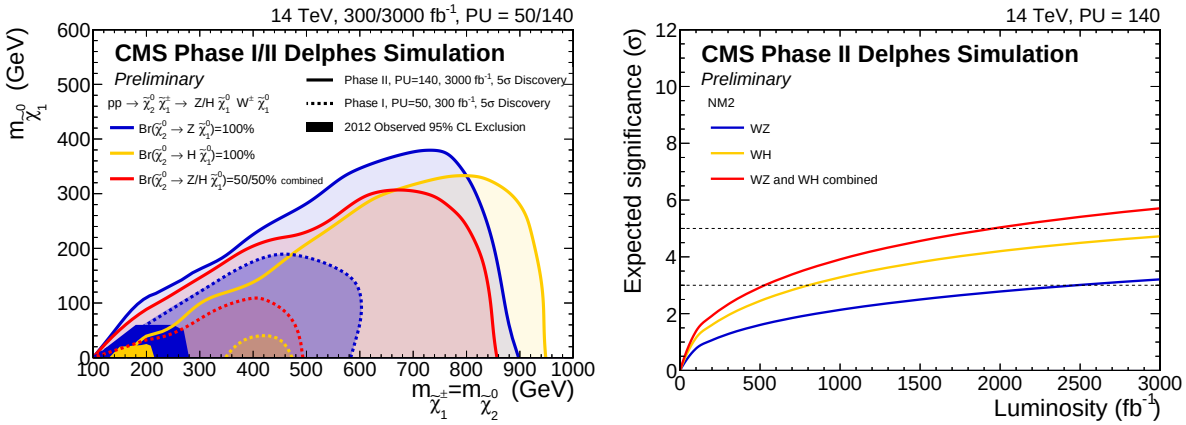

(a) (b)

Figure 24: (a) Contours for 5σ discovery of $\widetilde{\chi}_1^{\pm}\widetilde{\chi}_2^0$ production are shown in the simplified model parameter space of $m_{\widetilde{\chi}_1^{\pm}} = m_{\widetilde{\chi}_2^0}$ versus $m_{\widetilde{\chi}_1^0}$ for three different branching fraction assumptions of $\mathcal{B}(\widetilde{\chi}_2^0 \to Z\widetilde{\chi}_1^0) = 100\%$, $\mathcal{B}(\widetilde{\chi}_2^0 \to H\widetilde{\chi}_1^0) = 100\%$, and $\mathcal{B}(\widetilde{\chi}_2^0 \to Z\widetilde{\chi}_1^0) = \mathcal{B}(\widetilde{\chi}_2^0 \to H\widetilde{\chi}_1^0) = 50\%$. For the last assumption, the sensitivity is obtained from the combination of the WZ + $E_{\mathrm{T}}^{\mathrm{miss}}$ and WH + $E_{\mathrm{T}}^{\mathrm{miss}}$ searches. The excluded regions based on the 8 TeV data collected in 2012 are also shown. (b) The discovery sensitivities for the natural model NM2 from the combination of the WZ + $E_{\mathrm{T}}^{\mathrm{miss}}$ and WH + $E_{\mathrm{T}}^{\mathrm{miss}}$ searches are also shown as a function of the integrated luminosity, together with the sensitivities from the individual WZ + $E_{\mathrm{T}}^{\mathrm{miss}}$ and WH + $E_{\mathrm{T}}^{\mathrm{miss}}$ searches.

14 Discovery stories

Here, we discuss what we will learn in the LHC Run 2+3 and with the HL-LHC based on nine different analyses assuming that one of the five benchmark models defined in Section 4 is realized in nature (see Table 1). The stories below are meant as examples of new possibilities for discovery that the HL-LHC provides, rather than exhaustive studies of each model, and provide further motivation for CMS Phase II detector upgrades.

14.1 Natural models

In the three natural SUSY inspired models (NM1, NM2, and NM3) that we studied, the gluino mass is about 1.7 TeV, and the $\widetilde{\mathrm{t}}_1$ and $\widetilde{\mathrm{b}}_1$ masses are about 1.1 TeV, while the first- and second-generation squarks have their masses around 3 TeV. Therefore, the gluino decays to either $\mathrm{t}\widetilde{\mathrm{t}}_1$ or $\mathrm{b}\widetilde{\mathrm{b}}_1$. The branching fractions of $\widetilde{\mathrm{t}}_1$ and $\widetilde{\mathrm{b}}_1$ vary among these models, but the final state of gluino pair production will include a total of four b-quarks either directly coming from gluino decays or from $\widetilde{\mathrm{t}}_1/\widetilde{\mathrm{b}}_1$. The three models differ in the weakly interacting SUSY particle sector as discussed in detail in Section 4. These differences drastically change how $\widetilde{\mathrm{t}}_1/\widetilde{\mathrm{b}}_1$ decay. In NM1, we expect to see long cascade decays of $\widetilde{\mathrm{t}}_1/\widetilde{\mathrm{b}}_1$ and numerous leptons from $\widetilde{\chi}_2^0/\widetilde{\chi}_1^{\pm}$ decays, while in NM2 we expect to see gauge bosons (W, Z, and H) in $\widetilde{\chi}_2^0/\widetilde{\chi}_1^{\pm}$ decays. In NM3 we expect that $\widetilde{\mathrm{t}}_1/\widetilde{\mathrm{b}}_1$ decay predominantly into a top quark and higgsino-like mass-degenerate $\widetilde{\chi}_{1,2}^0/\widetilde{\chi}_1^{\pm}$.

We expect to have a $\geq 5\sigma$ discovery of gluino signatures in the all-hadronic M_{T2} search with $\geq$3 b-tags (Section 7) in the cases of NM2 and NM3, and in the trilepton + b-tag search (Section 12) for any natural models with $\leq 300\,\mathrm{fb}^{-1}$ of data. The single-lepton search targeted for $\widetilde{\mathrm{t}}_1\widetilde{\mathrm{t}}_1^*$ production also has strong sensitivity to each of the natural SUSY models and yields 5σ observation with less than $300\,\mathrm{fb}^{-1}$ of data (Section 9). However, it is challenging to confirm the

observation of direct production of $\widetilde{t}_1$ pairs due to sizable intrinsic SUSY background contributions from $\widetilde{g}\widetilde{g}$, $\widetilde{q}\widetilde{g}$, and $\widetilde{b}_1\widetilde{b}_1$ production. In addition, the sparticle spectrum below the $\widetilde{t}_1$ mass is too rich in these models to allow for a large enough rate of $\widetilde{t}_1\widetilde{t}_1^*$ production with $\widetilde{t}_1 \to t\widetilde{\chi}_1^0$ that this search is optimized for.

The richness of the spectrum below the $\widetilde{t}_1$ and $\widetilde{b}_1$ masses in NM1 and NM2 is likely to lead to a variety of interesting measurements with the full HL-LHC dataset. In this document we focus on only a few of these as examples. In NM1, we will be able to observe an edge in the invariant mass distribution of two opposite-sign same-flavor leptons when they originate from the $\widetilde{\chi}_2^0$ decay via $\widetilde{\chi}_2^0 \to \ell\widetilde{\ell} \to \ell^+\ell^-\widetilde{\chi}_1^0$, as discussed in Section 11, and this edge mass will give information on the $\widetilde{\chi}_{1,2}^0$ and $\widetilde{\ell}_L$ masses through $m_{\text{edge}} = \sqrt{(m^2_{\widetilde{\chi}_2^0} - m^2_{\widetilde{\ell}})(m^2_{\widetilde{\ell}} - m^2_{\widetilde{\chi}_1^0})}/m_{\widetilde{\ell}}$. In models like NM2, the WH + E_T^{miss} search may observe a signal coming from direct $\widetilde{\chi}_1^\pm\widetilde{\chi}_2^0$ production, in which $\widetilde{\chi}_1^\pm$ decays into $W\widetilde{\chi}_1^0$ and $\widetilde{\chi}_2^0$ decays into $H\widetilde{\chi}_1^0$, with 3000 fb^{-1} of data if the mass difference between the wino-like $\widetilde{\chi}_1^\pm/\widetilde{\chi}_2^0$ and the bino-like $\widetilde{\chi}_1^0$ is sufficiently large, as discussed in Section 13.2. Our specific implementation of NM2 has a bino mass of about 200 GeV, a wino mass of about 535 GeV, and a branching fraction of 88% for $\widetilde{\chi}_1^\pm\widetilde{\chi}_2^0$ into WH + E_T^{miss}. A 100 GeV heavier wino at the same branching fraction would be discoverable. In addition, the WZ + E_T^{miss} search with 3000 fb^{-1} of data can provide an about 3σ evidence of a signal as well (Section 13.1), and a $\geq 5\sigma$ discovery of $\widetilde{\chi}_1^\pm\ \widetilde{\chi}_2^0$ production is possible if the analyses of both final states are combined.

The HL-LHC would thus be able to distinguish between these three types of models. The crucial distinguishing features are a characteristic dilepton edge for NM1, a WZ and/or WH + E_T^{miss} observation for NM2, and an excess of events at very large M_{T2} for NM3. By distinguishing between these different types of models the HL-LHC program would elucidate the gross features of the spectrum of weakly interacting particles.

14.2 Stau coannihilation model

In the stau coannihilation (STC) model, the $\widetilde{t}_1$ and $\widetilde{b}_1$ masses are 882 and 1000 GeV, respectively, and we expect an observation of their direct production in the $b\bar{b}$ + E_T^{miss} final state with 1000 fb^{-1} (Section 8) and $t\bar{t}$ + E_T^{miss} final state with 900 fb^{-1} (Section 9). In addition, we expect an observation in the trilepton + 2–3 b-tag final state with about 400 fb^{-1} (Section 12). The combination of these indicates a natural SUSY spectrum with both $\widetilde{t}_1$ and $\widetilde{b}_1$ at 1 TeV scale, and a complex weakly interacting SUSY sector. Studies of exclusive final states as performed in, e.g., multilepton searches [19], would unveil the weakly interacting SUSY sector.

Over 80% of signal events in the sbottom search originate from $\widetilde{b}_1 \to b\widetilde{\chi}_1^0$, and measurements of M_{CT} spectra would allow the determination of the endpoint of the M_{CT} specturm, M_{CT}^{max}, with about 10% accuracy. This M_{CT}^{max} gives some clue about the SUSY particle spectrum through $M_{CT}^{\text{max}} \approx (m^2_{\widetilde{b}_1} - m^2_{\widetilde{\chi}_1^0})/m_{\widetilde{b}_1}$ [56, 57]. In addition, an excess in the H_T-H_T^{miss} search with $\geq$2 b-tags with $\approx$ 3000 fb^{-1} gives a strong hint of the existence of the heavy colored sparticles at about 3 TeV.

14.3 Stop coannihilation model

In the stop coannihilation (STOC) model, we expect to observe some excess with 300 fb^{-1} in the monojet search, and 3000 fb^{-1} from HL-LHC running can almost lead to 5σ observation (Section 10). We also expect observation of the $t\bar{t}$ + E_T^{miss} final state in the H_T-H_T^{miss} search with $\geq$2 b-tags and in the single-lepton search targeted for this signature as discussed in Sections 6

and 9, respectively. The null observation in searches for the $b\bar{b}$ + E_T^{miss} final state (Section 8) and in H_T-H_T^{miss} searches with $\geq$4 b-tags supports the hypothesis of the gluino decaying into a top quark and a top squark degenerate with the LSP, as in the STOC model. The HL-LHC would thus indicate the existence of a viable dark matter candidate that is consistent with the measured relic density [30, 31]. In addition, further studies of kinematic distributions, e.g., the H_T distribution, in the HL-LHC dataset would suggest the existence of the first- and second-generation squarks with masses of about 3.4 TeV in addition to the gluinos, giving further information about a more complete SUSY spectrum.

15 Conclusions

The discovery of a Higgs boson at 125 GeV has given new urgency to the question of how the electroweak scale is stabilized against short-distance quantum corrections that must inevitably arise in the SM. Addressing this question is one of the major goals of the LHC program for the next decade and beyond. The solution can in principle be either accidental or natural. Supersymmetry provides one, but by no means the only, approach to resolving the gauge hierarchy problem.

If a SUSY spectrum of any kind emerges from the LHC program, we will have finally broken through to beyond-the-SM physics in accelerator experiments. The studies presented here show that a broad range of searches will provide a way to discover and characterize what may be a very complex spectrum. In the absence of reconstructed mass peaks, the pattern of such results provides essential information for characterizing the different sectors of such a spectrum. Natural SUSY models are expected to produce signals in channels with gluinos, third-generation squarks, and higgsinos. Because the decays of the third-generation squarks would be sensitive to the arrangement of the electroweak and slepton sectors, the observed pattern of signals and their individual kinematic distributions will provide crucial information for identifying the underlying spectrum.

In this document, we have presented studies on the discovery potential of SUSY particles in the high-luminosity running of the LHC with 3000 fb^{-1} of integrated luminosity. We have investigated five benchmark full-spectrum SUSY models and their signatures, and pointed out the reach of the CMS experiment to test these models in nine different analyses targeting different final states. Studies based on these models provide interesting illustrations of how the HL-LHC can unveil the SUSY particle spectrum.

We have also investigated the discovery reach for direct chargino-neutralino ($\widetilde{\chi}_1^{\pm}\widetilde{\chi}_2^0$) production in the WZ + E_T^{miss} and WH + E_T^{miss} final states based on the simplified SUSY model. The cross section of direct $\widetilde{\chi}_1^{\pm}\widetilde{\chi}_2^0$ production is low compared to the direct production of colored SUSY particles of comparable masses, therefore the potential discovery reach for such process will especially profit from the high-luminosity upgrade of the LHC. With 3000 fb^{-1} we will be able to discover $\tilde{\chi}_1^{\pm}$ and $\tilde{\chi}_2^0$ masses up to 950 GeV with a significance of $\geq 5\sigma$.

The extension of the discovery reach from 300 fb^{-1} to 3000 fb^{-1} is dramatic, increasing the discovery region more than 10-fold as shown in Fig. 22(a) for the WH + E_T^{miss} final state. Those physics capabilities will not be fully realized if the CMS detector does not maintain its superb performance through the HL-LHC period. We demonstrated for the WH + E_T^{miss} final state that accumulating 1000 fb^{-1} of data with a degraded detector extends the discovery reach only marginally beyond the 300 fb^{-1} discovery reach, while with 1000 fb^{-1} of data accumulated with the Phase II detector, the discovery reach is extended substantially.

A Detailed model information

This appendix contains detailed information about the models. The masses of the relevant SUSY particles are displayed in Fig. 2 and given in Table 15. The cross sections of main SUSY particle production processes and the branching fractions of the most relevant SUSY particles are presented in Tables 16 and 17, respectively.

Table 15: Overview of the most relevant sparticle masses for the models NM1, NM2, NM3, STC, and STOC. $\widetilde{q}$ denotes the first two generation squarks, and their average mass is listed.

Sparticle	Mass (GeV)				
	NM1	NM2	NM3	STC	STOC
$\widetilde{g}$	1686	1686	1686	3007	2132
$\widetilde{b}_1$	1177	1177	1163	1000	2374
$\widetilde{t}_1$	1092	1090	1144	882	402
$\widetilde{t}_2$	1874	1875	1910	1446	2393
$\widetilde{q}$	3025	3025	3026	3189	3417
$\widetilde{\ell}_L^{\pm}$	432	3000	3000	318	3037
$\widetilde{\ell}_R^{\pm}$	3000	3000	3000	203	2997
$\widetilde{\tau}_1$	427	2999	3000	194	2806
$\widetilde{\chi}_1^0$	419	199	195	187	396
$\widetilde{\chi}_2^0$	515	535	208	228	763
$\widetilde{\chi}_3^0$	603	607	557	609	2913
$\widetilde{\chi}_4^0$	644	656	837	617	2915
$\widetilde{\chi}_1^{\pm}$	512	534	201	228	763
$\widetilde{\chi}_2^{\pm}$	642	656	837	618	2915

Table 16: Cross sections of main SUSY particle production processes for the models NM1, NM2, NM3, STC, and STOC. The cross sections are calculated at the next-to-leading-order accuracy [62–64]. The cross sections below 0.01 fb are not listed.

Process	Cross section (fb)				
	NM1	NM2	NM3	STC	STOC
$\widetilde{g}\widetilde{g}$	5.4	5.4	5.4	0.007	0.53
$\widetilde{q}\widetilde{g}$	2.0	2.0	2.0	0.05	0.30
$\widetilde{q}\widetilde{q}$, $\widetilde{q}\widetilde{q}^*$	0.14	0.14	0.14	0.07	0.03
$\widetilde{b}_1\widetilde{b}_1^*$	2.6	2.6	2.8	8.3	-
$\widetilde{t}_1\widetilde{t}_1^*$	4.4	4.4	3.1	19	2110
$\widetilde{\chi}_1^{\pm}\widetilde{\chi}_1^0$	1.1	0.2	520	11	-
$\widetilde{\chi}_1^{\pm}\widetilde{\chi}_2^0$	29	22	460	1104	5.5
$\widetilde{\chi}_1^0\widetilde{\chi}_2^0$	-	-	258	0.02	-
$\widetilde{\chi}_1^+\widetilde{\chi}_1^-$	15	11	278	553	2.6
$\widetilde{\ell}^+\widetilde{\ell}^-$	3.3	-	-	34	-
$\widetilde{\ell}^+\widetilde{\nu}$, $\widetilde{\ell}^-\widetilde{\nu}^*$	12	-	-	32	-
$\widetilde{\nu}\widetilde{\nu}^*$	3.3	-	-	13	-

Table 17: Main branching fractions of SUSY particles for the models NM1, NM2, NM3, STC, and STOC.

Decay	Branching fraction				
	NM1	**NM2**	**NM3**	**STC**	**STOC**
$\widetilde{g} \to \widetilde{t}_1\bar{t}, \widetilde{t}_1^*t$	59%	60%	53%	28%	50%
$\widetilde{g} \to \widetilde{b}_1\bar{b}, \widetilde{b}_1^*b$	41%	40%	47%	28%	50%
$\widetilde{g} \to \widetilde{t}_2\bar{t}, \widetilde{t}_2^*t$	-	-	-	22%	-
$\widetilde{g} \to \widetilde{b}_2\bar{b}, \widetilde{b}_2^*b$	-	-	-	21%	-
$\widetilde{t}_1 \to t\widetilde{\chi}_1^0$	0.6%	1.5%	39%	20%	-
$\widetilde{t}_1 \to t\widetilde{\chi}_2^0$	13%	13%	41%	5.4%	-
$\widetilde{t}_1 \to t\widetilde{\chi}_3^0$	22%	23%	1.3%	20%	-
$\widetilde{t}_1 \to t\widetilde{\chi}_4^0$	30%	30%	5.5%	9.2%	-
$\widetilde{t}_1 \to b\widetilde{\chi}_1^+$	16%	12%	2.1%	12%	-
$\widetilde{t}_1 \to b\widetilde{\chi}_2^+$	18%	21%	11%	34%	-
$\widetilde{t}_1 \to c\widetilde{\chi}_1^0$	-	-	-	-	99%
$\widetilde{b}_1 \to b\widetilde{\chi}_1^0$	1.5%	1.0%	1.3%	67%	-
$\widetilde{b}_1 \to b\widetilde{\chi}_2^0$	11%	10%	1.0%	2.2%	5.7%
$\widetilde{b}_1 \to b\widetilde{\chi}_3^0$	0.6%	0.6%	0.4%	8.2%	-
$\widetilde{b}_1 \to b\widetilde{\chi}_4^0$	4.5%	5.7%	5.7%	7.6%	-
$\widetilde{b}_1 \to t\widetilde{\chi}_1^-$	32%	34%	80%	3.4%	11%
$\widetilde{b}_1 \to t\widetilde{\chi}_2^-$	49%	48%	12%	12%	-
$\widetilde{b}_1 \to W^-\widetilde{t}_1$	0.4%	0.7%	-	$< 0.1\%$	65%
$\widetilde{b}_1 \to b\widetilde{g}$	-	-	-	-	18%
$\widetilde{\chi}_1^+ \to \ell^+\widetilde{\nu}$	56%	-	-	-	-
$\widetilde{\chi}_1^+ \to \nu\widetilde{\ell}^+$	43%	-	-	100% (only $\nu_\tau\widetilde{\tau}_1^+$)	-
$\widetilde{\chi}_1^+ \to W^+\widetilde{\chi}_1^0$	1.8%	100%	-	-	-
$\widetilde{\chi}_1^+ \to q\bar{q}'\widetilde{\chi}_1^0$	-	-	70%	-	-
$\widetilde{\chi}_1^+ \to \ell^+\nu\widetilde{\chi}_1^0$	-	-	30%	-	-
$\widetilde{\chi}_1^+ \to \widetilde{t}_1\bar{b}$	-	-	-	-	100%
$\widetilde{\chi}_2^0 \to \ell^+\widetilde{\ell}^-, \ell^-\widetilde{\ell}^+$	59%	-	-	100%	-
$\widetilde{\chi}_2^0 \to \widetilde{\nu}\bar{\nu}, \widetilde{\nu}^*\nu$	41%	-	-	-	-
$\widetilde{\chi}_2^0 \to Z\widetilde{\chi}_1^0$	$< 0.1\%$	12%	-	-	-
$\widetilde{\chi}_2^0 \to H\widetilde{\chi}_1^0$	-	88%	-	-	-
$\widetilde{\chi}_2^0 \to q\bar{q}\widetilde{\chi}_1^0$	-	-	56%	-	-
$\widetilde{\chi}_2^0 \to \ell^+\ell^-\widetilde{\chi}_1^0$	-	-	10%	-	-
$\widetilde{\chi}_2^0 \to \nu\bar{\nu}\widetilde{\chi}_1^0$	-	-	21%	-	-
$\widetilde{\chi}_2^0 \to q\bar{q}'\widetilde{\chi}_1^\pm$	-	-	8.8%	-	-
$\widetilde{\chi}_2^0 \to \ell^+\nu\widetilde{\chi}_1^-, \ell^-\bar{\nu}\widetilde{\chi}_1^+$	-	-	4.0%	-	-
$\widetilde{\chi}_2^0 \to \widetilde{t}_1\bar{t}, \widetilde{t}_1^*t$	-	-	-	-	100%

References

[1] S. P. Martin, "A Supersymmetry Primer", arXiv:hep-ph/9709356v6.

[2] J. Wess and B. Zumino, "Supergauge transformations in four dimensions", *Nucl. Phys. B* **70** (1974) 39, doi:10.1016/0550-3213(74)90355-1.

[3] H. P. Nilles, "Supersymmetry, Supergravity and Particle Physics", *Phys. Reports* **110** (1984) 1, doi:10.1016/0370-1573(84)90008-5.

[4] H. E. Haber and G. L. Kane, "The Search for Supersymmetry: Probing Physics Beyond the Standard Model", *Phys. Reports* **117** (1987) 75, doi:doi:10.1016/0370-1573(85)90051-1.

[5] R. Barbieri, S. Ferrara, and C. A. Savoy, "Gauge Models with Spontaneously Broken Local Supersymmetry", *Phys. Lett. B* **119** (1982) 343, doi:10.1016/0370-2693(82)90685-2.

[6] S. Dawson, E. Eichten, and C. Quigg, "Search for Supersymmetric Particles in Hadron - Hadron Collisions", *Phys. Rev. D* **31** (1985) 1581, doi:10.1103/PhysRevD.31.1581.

[7] M. Papucci, J. T. Ruderman, and A. Weiler, "Natural SUSY endures", *JHEP* **1209** (2012) 035, doi:10.1007/JHEP09(2012)035, arXiv:1110.6926.

[8] CMS Collaboration, "Projected Performance of an Upgraded CMS Detector at the LHC and HL-LHC: Contribution to the Snowmass Process", arXiv:1307.7135.

[9] CMS Collaboration, "Study of the Discovery Reach in Searches for Supersymmetry at CMS with 3000 fb^{-1}", CMS Physics Analysis Summary CMS-PAS-FTR-13-014, 2013.

[10] ATLAS Collaboration, "Prospects for benchmark Supersymmetry searches at the high luminosity LHC with the ATLAS Detector", ATL-PHYS-PUB-2013-011, 2013.

[11] ATLAS Collaboration, "Search for Supersymmetry at the high luminosity LHC with the ATLAS experiment", ATL-PHYS-PUB-2014-010, 2014.

[12] J. Alwall, P. Schuster, and N. Toro, "Simplified models for a first characterization of new physics at the LHC", *Phys. Rev.* **D 79** (2009) 075020, doi:10.1103/PhysRevD.79.075020, arXiv:0810.3921.

[13] D. Alves et al., "Simplified models for LHC new physics searches", *J. Phys.* **G 39** (2012) 105005, doi:10.1088/0954-3899/39/10/105005, arXiv:1105.2838.

[14] A. Djouadi, S. Rosier-Lees et al., "The Minimal Supersymmetric Standard Model: Group Summary Report", arXiv:hep-ph/9901246.

[15] C. F. Berger, J. S. Gainer, J. L. Hewett, and T. G. Rizzo, "Supersymmetry Without Prejudice", *JHEP* **0902** (2009) 023, doi:10.1088/1126-6708/2009/02/023, arXiv:0812.0980.

[16] S. S. AbdusSalam et al., "Fitting the phenomenological MSSM", *Phys. Rev.* **D 81** (2010) 095012, doi:10.1103/PhysRevD.81.095012, arXiv:0904.2548.

[17] CMS Collaboration, "Search for supersymmetry in pp collisions at in events with a single lepton, large jet multiplicity, and multiple b jets", *Phys. Lett. B* **733** (2014), no. 0, 328, doi:http://dx.doi.org/10.1016/j.physletb.2014.04.023.

[18] CMS Collaboration, "Search for supersymmetry in hadronic final states using M_{T2} with the CMS detector at $\sqrt{s} = 8$ TeV", CMS Physics Analysis Summary CMS-PAS-SUS-13-019, 2013.

[19] CMS Collaboration, "Searches for electroweak production of charginos, neutralinos, and sleptons decaying to leptons and W, Z, and Higgs bosons in pp collisions at 8 TeV", *Eur. Phys. J.* **C 74** (2014), no. 9, 3036, doi:10.1140/epjc/s10052-014-3036-7, arXiv:1405.7570.

[20] A. Djouadi, J.-L. Kneur, and G. Moultaka, "SuSpect: A Fortran code for the Supersymmetric and Higgs particle spectrum in the MSSM", *Comput. Phys. Commun.* **176** (2007) 426, doi:10.1016/j.cpc.2006.11.009, arXiv:hep-ph/0211331.

[21] B. Allanach, "SOFTSUSY: a program for calculating supersymmetric spectra", *Comput. Phys. Commun.* **143** (2002) 305, doi:10.1016/S0010-4655(01)00460-X, arXiv:hep-ph/0104145.

[22] A. Djouadi, M. Muhlleitner, and M. Spira, "Decays of Supersymmetric Particles: the program SUSY-HIT (SUspect-SdecaY-Hdecay-InTerface)", *Acta Phys. Polon.* **B 38** (2007) 635, arXiv:hep-ph/0609292.

[23] J. Alwall et al., "MadGraph 5 : going beyond", *JHEP* **1106** (2011) 128, doi:10.1007/JHEP06(2011)128, arXiv:1106.0522.

[24] J. Alwall et al., "The automated computation of tree-level and next-to-leading order differential cross sections, and their matching to parton shower simulations", *JHEP* **1407** (2014) 079, doi:10.1007/JHEP07(2014)079, arXiv:1405.0301.

[25] T. Sjöstrand, S. Mrenna, and P. Skands, "PYTHIA 6.4 physics and manual", *JHEP* **05** (2006) 026, doi:10.1088/1126-6708/2006/05/026, arXiv:hep-ph/0603175.

[26] DELPHES 3 Collaboration, "DELPHES 3, A modular framework for fast simulation of a generic collider experiment", *JHEP* **1402** (2014) 057, doi:10.1007/JHEP02(2014)057, arXiv:1307.6346.

[27] Planck Collaboration, "Planck 2013 results. XVI. Cosmological parameters", *Astron.Astrophys.* (2014) doi:10.1051/0004-6361/201321591, arXiv:1303.5076.

[28] C. L. Bennett et al., "Nine-year Wilkinson Microwave Anisotropy Probe (WMAP) Observations: Final Maps and Results", *Astrophysical Journal, Supplement* **208** (2013) 20, doi:10.1088/0067-0049/208/2/20, arXiv:1212.5225.

[29] O. Buchmueller et al., "Likelihood functions for supersymmetric observables in frequentist analyses of the CMSSM and NUHM1", *Eur. Phys. J.* **C 64** (2009) 391, doi:10.1140/epjc/s10052-009-1159-z, arXiv:0907.5568.

[30] J. R. Ellis, K. A. Olive, and Y. Santoso, "Calculations of neutralino stop coannihilation in the CMSSM", *Astropart. Phys.* **18** (2003) 395, doi:10.1016/S0927-6505(02)00151-2, arXiv:hep-ph/0112113.

[31] J. Ellis, K. A. Olive, and J. Zheng, "The Extent of the Stop Coannihilation Strip", arXiv:1404.5571.

[32] CMS Collaboration, "Search for new physics in the multijet and missing transverse momentum final state in proton-proton collisions at $\sqrt{s} = 8$ TeV", *JHEP* **1406** (2014) 055, doi:10.1007/JHEP06(2014)055, arXiv:1402.4770.

[33] CMS Collaboration, "Search for gluino mediated bottom- and top-squark production in multijet final states in pp collisions at 8 TeV", *Phys. Lett.* **B 725** (2013) 243, doi:10.1016/j.physletb.2013.06.058, arXiv:1305.2390.

[34] CMS Collaboration, "Search for direct production of bottom squark pairs", CMS Physics Analysis Summary CMS-PAS-SUS-13-018, 2013.

[35] CMS Collaboration, "Search for top-squark pair production in the single-lepton final state in pp collisions at $\sqrt{s} = 8$ TeV", *Eur. Phys. J.* **C 73** (2013) 2677, doi:10.1140/epjc/s10052-013-2677-2, arXiv:1308.1586.

[36] CMS Collaboration, "Search for top squarks decaying to a charm quark and a neutralino in events with a jet and missing transverse momentum", CMS Physics Analysis Summary CMS-PAS-SUS-13-009, 2013.

[37] CMS Collaboration, "CMS Technical Design Report for the Phase 1 Upgrade of the Hadron Calorimeter", CMS Technical Design Report CERN-LHCC-2012-015, CMS-TDR-10, 2012.

[38] CMS Collaboration, "CMS Technical Design Report for the Pixel Detector Upgrade", CMS Technical Design Report CERN-LHCC-2012-016, CMS-TDR-11, 2012.

[39] CMS Collaboration, "CMS Technical Design Report for the Level-1 Trigger Upgrade", CMS Technical Design Report CERN-LHCC-2013-011, CMS-TDR-12, 2013.

[40] M. Cacciari and G. P. Salam, "Pileup subtraction using jet areas", *Phys. Lett.* **B 659** (2008) 119, doi:10.1016/j.physletb.2007.09.077, arXiv:0707.1378.

[41] J. Anderson et al., "Snowmass Energy Frontier Simulations", arXiv:1309.1057.

[42] A. Avetisyan et al., "Methods and Results for Standard Model Event Generation at $\sqrt{s} =$ 14 TeV, 33 TeV and 100 TeV Proton Colliders (A Snowmass Whitepaper)", arXiv:1308.1636.

[43] A. Avetisyan et al., "Snowmass Energy Frontier Simulations using the Open Science Grid (A Snowmass 2013 whitepaper)", arXiv:1308.0843.

[44] L. Moneta et al., "The RooStats Project", *PoS* **ACAT2010** (2010) 057, arXiv:1009.1003.

[45] R. D. Cousins, J. T. Linnemann, and J. Tucker, "Evaluation of three methods for calculating statistical significance when incorporating a systematic uncertainty into a test of the background-only hypothesis for a Poisson process", *Nucl. Instrum. Methods Phys. Res., Sect. A* **595** (2008) 480, doi:10.1016/j.nima.2008.07.086, arXiv:physics/0702156.

[46] K. Cranmer, "Statistical Challenges for Searches for New Physics at the LHC", in *Statistical Problems in Particle Physics, Astrophysics and Cosmology*, p. 112. 2006. arXiv:physics/0511028. doi:10.1142/9781860948985_0026.

[47] J. Linnemann, "Measures of Significance in HEP and Astrophysics", in *Statistical Problems in Particle Physics, Astrophysics, and Cosmology*, p. 35. 2003. arXiv:physics/0312059.

[48] ATLAS and CMS Collaborations, "Procedure for the LHC Higgs boson search combination in Summer 2011", ATL-PHYS-PUB-2011-011, CMS NOTE-2011/005, 2011.

[49] CMS Collaboration, "Search for new physics with jets and missing transverse momentum in pp collisions at $\sqrt{s} = 7$ TeV", *JHEP* **08** (2011) 155, doi:10.1007/JHEP08(2011)155, arXiv:1106.4503.

[50] CMS Collaboration, "Search for New Physics in the Multijet and Missing Transverse Momentum Final State in Proton-Proton Collisions at $\sqrt{s} = 7$ TeV", *Phys. Rev. Lett.* **109** (2012) 171803, doi:10.1103/PhysRevLett.109.171803, arXiv:1207.1898.

[51] CMS Collaboration, "Search for supersymmetry in events with b jets and missing transverse momentum at the LHC", *JHEP* **1107** (2011) 113, doi:10.1007/JHEP07(2011)113, arXiv:1106.3272.

[52] CMS Collaboration, "Search for supersymmetry in events with b-quark jets and missing transverse energy in pp collisions at 7 TeV", *Phys. Rev.* **D 86** (2012) 072010, doi:10.1103/PhysRevD.86.072010, arXiv:1208.4859.

[53] A. Barr, C. Lester, and P. Stephens, "A variable for measuring masses at hadron colliders when missing energy is expected; m_{T2}: the truth behind the glamour", *J. Phys.* **G 29** (2003) 2343, doi:10.1088/0954-3899/29/10/304, arXiv:arXiv:hep-ph/0304226.

[54] M. Burns, K. Kong, K. T. Matchev, and M. Park, "Using subsystem M_{T2} for complete mass determinations in decay chains with missing energy at hadron colliders", *JHEP* **0903** (2009) 143, doi:10.1088/1126-6708/2009/03/143, arXiv:arXiv:0810.5576.

[55] CMS Collaboration, "Search for supersymmetry in hadronic final states using M_{T2} in pp collisions at $\sqrt{s} = 7$ TeV", *JHEP* **1210** (2012) 018, doi:10.1007/JHEP10(2012)018, arXiv:1207.1798.

[56] D. Tovey, "On measuring the masses of pair-produced semi-invisibly decaying particles at hadron colliders", *JHEP* **0804** (2008) 034, doi:10.1088/1126-6708/2008/04/034, arXiv:arXiv:0802.2879.

[57] G. Polesello and D. R. Tovey, "Supersymmetric particle mass measurement with the boost-corrected contransverse mass", *JHEP* **1003** (2010) 030, doi:10.1007/JHEP03(2010)030, arXiv:0910.0174.

[58] Y. Bai, H.-C. Cheng, J. Gallicchio, and J. Gu, "Stop the top background of the stop search", *JHEP* **1207** (2012) 110, doi:10.1007/JHEP07(2012)110, arXiv:1203.4813.

[59] ATLAS Collaboration, "Search for pair-produced third-generation squarks decaying via charm quarks or in compressed supersymmetric scenarios in pp collisions at $\sqrt{s} = 8$ TeV with the ATLAS detector", *Phys. Rev.* **D 90** (2014) 052008, doi:10.1103/PhysRevD.90.052008, arXiv:1407.0608.

[60] CMS Collaboration, "Search for new physics in events with opposite-sign leptons, jets, and missing transverse energy in pp collisions at $\sqrt{s} = 7$ TeV", *Phys. Lett.* **B 718** (2013) 815, doi:10.1016/j.physletb.2012.11.036, arXiv:1206.3949.

[61] CMS Collaboration, "Search for physics beyond the standard model in events with two opposite-sign same-flavor leptons, jets, and missing transverse energy in pp collisions at $\sqrt{s} = 8$ TeV", CMS Physics Analysis Summary CMS-PAS-SUS-12-019, 2014.

[62] W. Beenakker, R. Hopker, M. Spira, and P. Zerwas, "Squark and gluino production at hadron colliders", *Nucl. Phys.* **B 492** (1997) 51, doi:10.1016/S0550-3213(97)80027-2, arXiv:hep-ph/9610490.

[63] W. Beenakker et al., "Stop production at hadron colliders", *Nucl. Phys.* **B 515** (1998) 3, doi:10.1016/S0550-3213(98)00014-5, arXiv:hep-ph/9710451.

[64] W. Beenakker et al., "Production of Charginos, Neutralinos, and Sleptons at Hadron Colliders", *Phys. Rev. Lett.* **83** (1999) 3780, doi:10.1103/PhysRevLett.83.3780, arXiv:hep-ph/9906298.